



**Politecnico  
di Torino**

**Politecnico di Torino**

Master of Science  
in Energy and Nuclear Engineering  
A.y. 2020/2021  
July 2021

**In-Containment Aerosol Source  
Term Behaviour- Analysis in  
Support of MYRRHA Safety  
Assessment**

Supervisors:  
Prof. Fabio Subba  
Eng. Dario Bisogni

Candidate:  
Judy Rosso

# Abstract

The Multi-purpose HYbrid Research Reactor for High-tech Applications, MYRRHA is being designed at SCK CEN since 1998. The MYRRHA programme aims at demonstrating the principle of the Accelerator Driven System (ADS), with the main objective to study the efficient transmutation of high-level nuclear waste, and at providing a flexible and multi-purpose irradiation facility. It features a pool type reactor with subcritical core fed by a linear accelerator to sustain the fission reactions via spallation. Lead-bismuth eutectic (LBE) is both the selected coolant and the spallation target material.

The present study is carried out in support to the safety assessment of MYRRHA. For this technology, one of the main safety concerns is related to the presence of radioactive impurities (namely radiotoxic isotope  $^{210}\text{Po}$ , activation product of bismuth) in the LBE coolant. The analysis postulates the accidental release of coolant into the primary containment of the reactor, with subsequent generation of an LBE aerosol source term. The aim is to assess the efficiency of removal of the airborne radioactive material by means of natural aerosol deposition processes (i.e. gravitational settling and diffusion by Brownian motion). The study is performed with the aerosol dynamics model implemented in MELCOR code.

A preliminary sensitivity analysis is performed with the release of a monodisperse aerosol source, to assess the influence of the initial particle size and mass of LBE released on the evolution of the suspended mass in the Primary Containment.

It is followed by an uncertainty analysis aimed at experimenting the statistical methodology and tools to derive a Figure Of Merit (FOM, i.e. the suspended mass of radioactive aerosol) value compliant with the 95/95 criterion and at quantifying the influence of selected input parameters on the output value of the FOM, by means of correlation coefficients.

The selected uncertain parameters are: Mass Median Diameter (MMD) and Geometric Standard Deviation (GSD) of the aerosol source, aerosol dynamic shape factor and LBE mass released at accident onset. The analysis shows a dominant influence of the LBE mass released on the FOM during the first hour after accident onset. It is followed by an increasing influence of the remaining parameters, which indicate the higher influence that the release of smaller sized particles (small MMD and high GSD) and the departure from the ideal spherical shape of the particles (dynamic shape factor higher than one) assume towards the end of a one-week transient. Overall, a significant decrease of the aerosol source term can be achieved by accounting for natural deposition phenomena in the primary containment. The value of the aerosol decontamination factor one week into the transient is about 100 for the limit value of the FOM obtained.

In the final part of the study, a potential mitigation strategy is investigated: it consists in the injection (into the reactor primary containment atmosphere) of a monodisperse source of non-radioactive aerosols to enhance radioactive LBE aerosol deposition. One week after accident onset, a reduction of the in-containment source term up to a factor 5 can be achieved if such mitigation strategy would be implemented.

## List of symbols

$A_{floor}$	surface of the floor
$A_{diff}$	total surface available for diffusion by Brownian motion
$C_m$	Cunningham slip correction factor
$c_m$	mean velocity of gas molecule
$d_a$	aerodynamic diameter
$d_e$	equivalent volume diameter
$d_g$	geometric mean diameter
$d_i, d_j$	diameter of the $i^{\text{th}}$ and $j^{\text{th}}$ particle
$d_p$	particle diameter
$F_D$	drag force
$F_{slip}$	slip correction factor
$g$	acceleration of gravity
$g_k(v, \eta_k)$	marginal mass fraction probability density function
$m$	number of sections
$m_i$	mass of particles in group $i$
$M$	total mass
$M_w$	molecular weight
$n_i$	number of particles in group $i$
$n$	sample size
$N$	total number of sections
$n(v, t)$	number of particles per unit volume whose volume lies in the range $[v, v+dv]$
$p$	percentile value
$Q_{l,k}(t)$	mass of component $k$ in section $l$ at time $t$
$Q_l(t)$	total mass of aerosol per unit volume of fluid in section $l$ at time $t$
$R$	universal gas constant
$R[n(v, t), v, t]$	removal rate
$R_{grav}$	removal rate for gravitational settling
$R_{diff}$	removal rate for deposition by Brownian motion
$S(v, t)$	source rate
$T$	atmosphere temperature
$V$	velocity of the particle
$V_c$	total volume of the chamber
$v, u$	particle mass
$v_0$	smallest particle mass
$v_{diff}$	diffusion deposition velocity

$v_{grav}$	gravitational deposition velocity
$\tilde{v}_k$	mean mass of component $k$ for generated particles of size $v$
$\bar{v}_k, \bar{u}_k$	mean mass of component $k$
$v_m$	largest particle mass
$x, y$	variables
$\alpha$	level of significant
$\beta(u, v)$	agglomeration coefficient
$\beta_B$	Brownian agglomeration coefficient
$\beta_{grav}$	Gravitational agglomeration coefficient
$\beta_i$	delayed neutron fraction of the $i^{\text{th}}$ isotope
$\delta_D$	diffusion boundary layer thickness
$\varepsilon_g$	gravitational collision efficiency
$\eta_k, \xi_k$	mass fraction
$\pi_p$	percentile values distribution
$\rho_0$	unit density
$\rho_g$	gas density
$\rho_p$	particle density
$\gamma$	agglomeration shape factor
$\eta$	viscosity of the fluid
$\lambda$	mean free path of the atmospheric gas
$\mu$	viscosity of atmospheric gas
$\sigma$	Boltzmann constant
$\chi$	dynamic shape factor

## List of abbreviations

ADS	Accelerator-Driven System
AMMD	Aerodynamic Mass Mean Diameters
CMD	Count Median Diameter
DF	Decontamination Factor
FOM	Figure Of Merit
GDE	General Dynamic Equation
GMMD	Geometric Mass Mean Diameter
GSD	Geometric Standard Deviation
HLM	Heavy Liquid Metal
LBE	Lead-Bismuth Eutectic
LBECs	LBE Conditioning System
MA	Minor Actinide
MMD	Mass Median Diameter
MOX	Mixed Oxide
MYRRHA	HYbrid Research Reactor for High-tech Applications
P&T	Partitioning and Transmutation
UQ	Uncertainty Quantification
SFR	Sodium-cooled Fast Reactor
SMR	Small Modular Reactor

# Table of Contents

<b>1 Introduction .....</b>	<b>1</b>
1.1 Status of nuclear power .....	1
1.2 Partitioning and transmutation.....	3
1.3 Accelerator-Driven Systems.....	4
1.4 MYRRHA.....	6
1.5 LBE and LBE conditioning system .....	7
1.6 Accident scenario .....	8
1.7 Aim of the study .....	9
<b>2 Modelling approach and tool.....</b>	<b>11</b>
2.1 Description of MELCOR core.....	11
2.2 Aerosol dynamics model implemented in MECOR .....	12
2.2.1 General Dynamic Equations .....	13
2.2.1.1 Agglomeration coefficient.....	16
2.2.1.2 Removal of particles.....	17
2.2.2 Main parameters characterizing aerosol physics .....	18
2.2.3 Assumptions and approximations.....	20
2.3 Primary containment model.....	21
<b>3 Sensitivity analysis with monodisperse aerosol source .....</b>	<b>22</b>
3.1 Objective of the analysis.....	22
3.2 Methodological approach .....	22
3.2.1 Values of the aerosol input parameters.....	23
3.3 Results .....	23
3.3.1 Influence of initial aerosol size.....	24
3.3.2 Influence of initial aerosol mass .....	28
3.3.3 Deposition on heat structures .....	30
3.4 Conclusions .....	31
<b>4 Uncertainty analysis with lognormal aerosol size distribution .....</b>	<b>33</b>
4.1 Objective of the analysis.....	34
4.2 Methodological approach .....	34
4.2.1 Statistical considerations .....	37
4.2.2 Selection of uncertain parameters.....	38
4.2.2.1 Particle size distribution .....	38

4.2.2.2	Dynamic shape factor .....	42
4.2.2.3	Agglomeration shape factor.....	42
4.2.2.4	LBE aerosol mass released .....	43
4.2.2.5	Diffusive layer boundary thickness .....	43
4.2.3	Range of variation and statistical distribution of uncertain parameters .	43
4.3	Results .....	44
4.3.1	Values of FOM .....	44
4.3.2	Correlation coefficients- Explanation and values.....	46
4.3.3	Higher order statistics .....	50
4.4	Conclusions .....	52
<b>5</b>	<b>Mitigation strategy .....</b>	<b>53</b>
5.1	Hypothesis to investigate .....	53
5.2	Reference case .....	53
5.3	Characteristics of the injection .....	54
5.4	Results .....	55
5.4.1	Injection 72h after the accident onset, in a wide range of size values....	55
5.4.2	Injection at different times.....	59
5.5	Conclusions .....	61
<b>6</b>	<b>Conclusions.....</b>	<b>62</b>
	<b>Bibliography.....</b>	<b>65</b>
	<b>Appendix A - Treatment of the aerosol size variable in MELCOR.....</b>	<b>68</b>

---

# Chapter 1

## Introduction

---

### 1.1 Status of nuclear power

Worldwide the net electricity generation is set to grow, especially in developing countries. The fastest growth in electricity generation is expected to come from renewable sources and natural gas, with a slower increase for nuclear power. Often not taken into account in these projections are the possible actions that could be taken to reduce carbon dioxide emissions: political and cultural factors will play a fundamental role in the choice of measures applied to achieve emission reduction goals. Therefore, concerns about climate change could have a strong influence on the development of new nuclear generating capacity. [1]

After the peak of new nuclear installations in the 1970s the number of new reactors has decreased, until the last couple of decades, when the number of new constructions slightly increased, with most of the new projects located in developing economies. The lifetimes of several power plants have been extended past the ones originally planned. As a consequence, the average age of the world's reactors has been rising. Therefore, the contribution of nuclear power to the transition to a sustainable energy system mostly relies on the prospects for new nuclear power projects. [2]

Several new advanced reactor technologies have been proposed or are in development and could have an important role in new investments in nuclear energy. New projects range in project size and in technical characteristics.

Some advanced nuclear technologies have the potential to serve purposes other electricity production such as produce process heat for industries or for water desalinization as well as being used in microgrids [3] and for actinide transmutation. Future nuclear reactors could compensate the intermittency of power production by renewable sources and they could, also, provide off-grid electricity and heat in isolated parts of the world. Additionally, the use of alternative fuels could in some cases allow the transmutation of isotopes previously considered as waste.

Several advanced designs for nuclear reactors are at different stages of development, in view of reaching commercialization. [1]

The current global nuclear energy system is mostly based on light water reactor (LWR) concepts and their fuel cycle. In LWRs the commonly used fuel is enriched uranium. A large fraction of spent fuel originating from a conventional nuclear power reactor contains long lived actinides, particularly neptunium, americium and curium. In recent years, interest has grown in the possibility of separating the longest lived and most radiotoxic isotopes present in the spent fuel and transmuting them into shorter lived radionuclides so that the management and eventual disposal of this radioactive waste is easier and less expensive. [4]

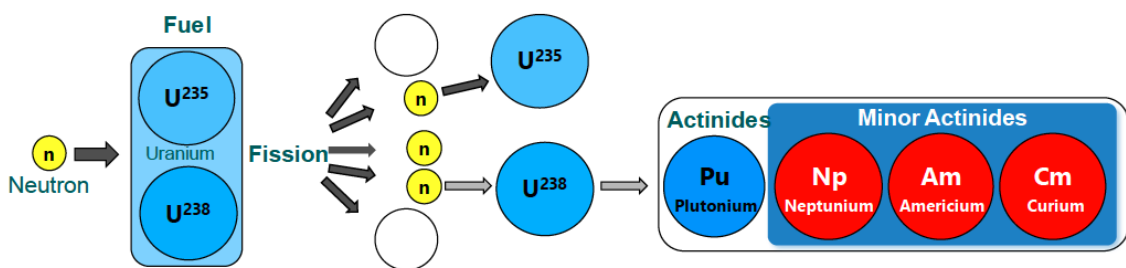


Figure 1.1- Fission reaction (source SCK CEN MYRRHA Project Team)

International efforts are underway to develop the future generation of nuclear energy systems, known as Generation IV (Gen IV). Nuclear energy research programs around the world have been developing concepts that could form the basis for Gen IV systems. A great effort in research and development surrounds the progress of the Gen IV concepts, aimed at having them available for international deployment by the year 2030. [5]

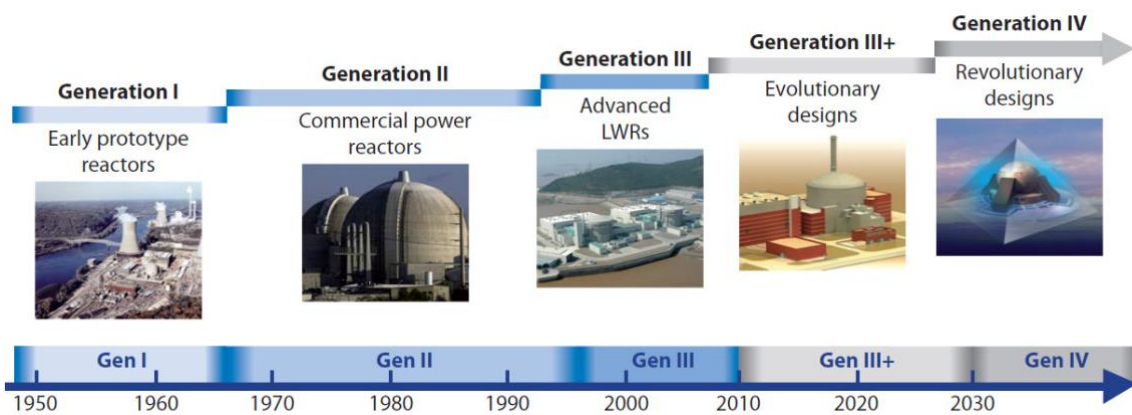


Figure 1.2- Generations of nuclear power [6]

## 1.2 Partitioning and transmutation

The two fuel cycles that are currently being exploited are the open fuel cycle that consists in the direct discharge of the spent fuel in geological disposals and the close fuel cycle that implements the reprocessing of spent fuel which allows the separation of isotopes that can be reused as fuel in the form of MOX (mixed oxide) fuel from isotopes to be sent to the geological disposal. The former presents problem with the lack of exploitation of the fuel but has economic advantages whereas the latter allows the reduction of the volume of the radioactive waste but still produces a certain amount of waste with a high level of radioactivity.

Several options to have a more efficient and sustainable fuel cycle are being investigated and developed. New technologies for partitioning and transmutation (P&T) of radioactive isotopes could play an important role in future scenarios, since they would allow for a reduction of the volume of high-level waste, therefore decreasing the burden on a geological disposal. As plutonium and the minor actinides (MA) are mainly responsible for the long-term radiotoxicity, when these nuclides are first removed from the irradiated fuel (partitioning) and then the fragmented by fission (transmutation), the remaining waste loses most of its long-term radiotoxicity. [7]

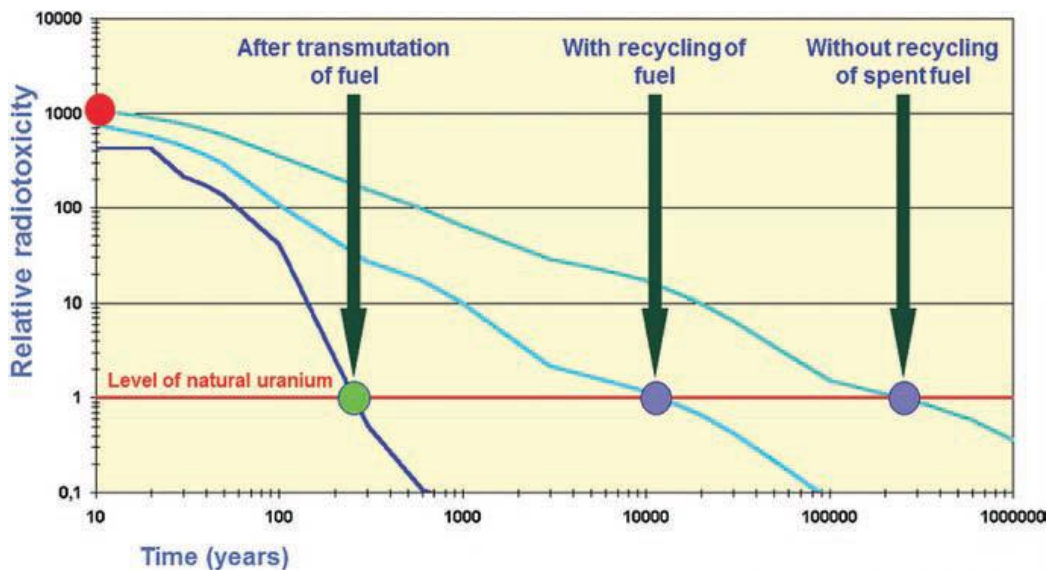


Figure 1.3- Radiotoxicity of radioactive waste [8]

The transmutation of plutonium and minor actinides requires high energy neutrons: it therefore calls for different operating conditions than the currently exploited light water technologies. The accelerator-driven systems are one of the nuclear technologies that would allow for the transmutation of long-lived radioactive waste.

### 1.3 Accelerator-Driven Systems

Accelerator-driven systems (ADS) are nuclear fission reactors with a subcritical core, that, thus, require an external neutron source for a stable neutron economy in the core. This source is provided by a spallation target coupled with an accelerator.

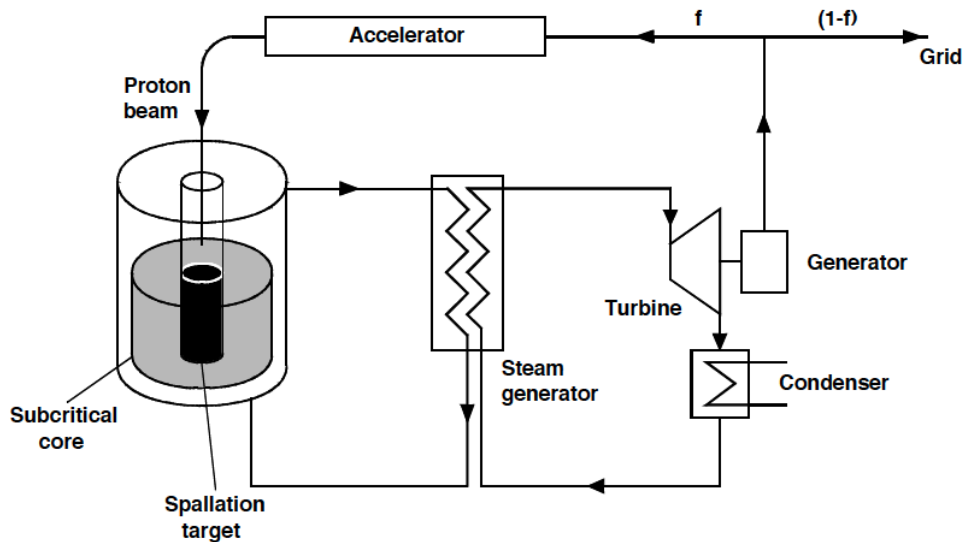


Figure 1.4- Concept of an accelerator-driven system [9]

The accelerator is the driver of the ADS. In most proposal for ADS applications, a proton accelerator can be found. The proton accelerator provides the high energy protons that are used in the spallation target to create neutrons which feed the subcritical core. The accelerator can both be a linear accelerator (linac) or a circular accelerator (cyclotron). Additionally, particle accelerators can be organized according to the time structure of their beam delivery: direct current (DC), a beam with no time structure; continuous wave (CW), where the beam is subdivided into small packets and delivered continuously to the target; pulsed, where the beam is subdivided into small packets and delivered with periodic interruptions. [8]

The spallation target is composed of solid or liquid metals. The spallation reaction occurs when a light projectile (proton, neutron, or light nucleus) with its high energy (from hundreds of MeV to several GeV) interacts with a heavy nucleus and causes the emission of a large number of hadrons (mostly neutrons) or fragments. It leads to a series of fast reactions called intranuclear cascade. The nuclei in their excited states decrease their energy level either through multi fragmentation, fission or evaporation. [10]

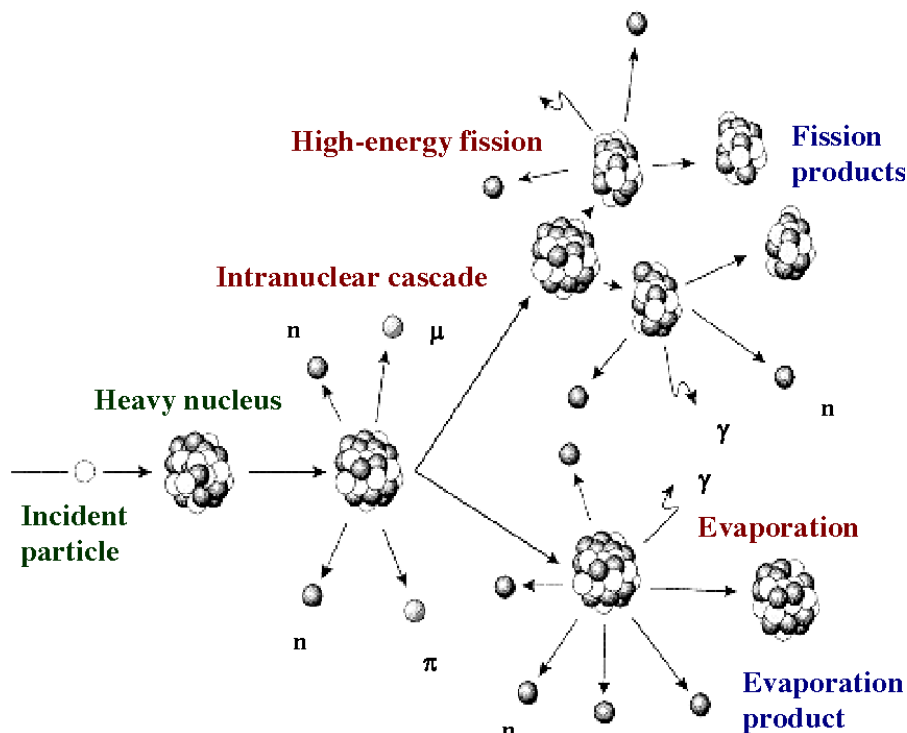


Figure 1.5- The scheme of spallation reaction [10]

The subcritical core does not have enough fissile material to reach criticality. Various types of nuclear fuel can be used, ranging from classical uranium fuel to advanced fuel heavily loaded with MA. The core can be designed to operated either with a thermal or fast neutron spectrum according to the final purpose of the reactor system.

As long as the system is operated with fast neutrons, the ADS systems can be used for nuclear waste transmutation. However, in order to get a concentrated and efficient transmutation of MAs, the subcritical operation of the system is a fundamental feature.

The fraction of MAs in the reactor core is limited by the reactor power variation. According to the composition of the fuel, the response of the systems varies in relation to the fraction of delayed neutron. A delayed neutron is a neutron that is released after the fission event by decay of one of the fission products, whereas a prompt neutron appears immediately after the fission event. Each fission process delivers neutrons, a fraction of which is delivered with a delay. The delayed neutron fraction for MAs is lower than for the uranium isotopes that compose classical fuel (Figure 1.6).

Nuclide	$\beta_I$ (pcm)
$^{235}\text{U}$	650
$^{238}\text{U}$	1480
$^{237}\text{Np}$	334
$^{238}\text{Pu}$	120
$^{239}\text{Pu}$	210
$^{240}\text{Pu}$	270
$^{241}\text{Pu}$	490
$^{242}\text{Pu}$	573
$^{241}\text{Am}$	113
$^{243}\text{Am}$	208
$^{242}\text{Cm}$	33
$^{244}\text{Cm}$	100

Figure 1.6- Delayed neutron fraction ( $\beta_I$ ) of selected isotopes [8]

The presence of delayed neutrons has an impact on the time constants of the time-dependent behaviour of a critical reactor. When the fraction of the delayed neutrons is too low (below 400-500 pcm), the time-constants associated with the exponential laws that describe the power excursion after a positive reactivity insertion become too small and the reactor becomes uncontrollable. It is thanks to the presence of delayed neutrons that the system becomes controllable.

In a critical reactor, the fraction of MAs will be limited to a few percent (2-5%). In a subcritical reactor a reactor core can contain up to 40-50% of MAs. Therefore, for a concentrated and efficient burning of MAs, the subcriticality is necessary. [8]

#### 1.4 MYRRHA

The Multi-purpose HYbrid Research Reactor for High-tech Applications, MYRRHA is being designed at SCK CEN since 1998. The MYRRHA programme is aimed at demonstrating the principle of the Accelerator Driven System (ADS) at such power levels that will allow to provide experience feedback scalable to an industrial demonstrator and will allow the study of efficient transmutation of high-level nuclear waste. [11] MYRRHA is positioned as a highly innovative and multidisciplinary research infrastructure that will be used for several other applications. It will be employed to ensure production of radioisotopes for medical applications, to carry out materials research and tests for the current and future nuclear fission reactors as well as nuclear fusion technology, to provide a multifunctional accelerator for fundamental and applied research. MYRRHA is also intended to be a technology demonstrator and an experimental technology test platform for Heavy Liquid Metal (HLM)-cooled reactor for Gen IV systems and HLM-based SMRs (Small and Medium Modular Reactors).

MYRRHA will integrate the three components of the ADS concept: proton accelerator, spallation target and sub-critical reactor.

The MYRRHA reactor will be able to operate in both sub-critical and critical mode, with a minimum power of 50 MWth. It is a pool type fast spectrum reactor with LBE (Lead-Bismuth Eutectic, composition: 44.5 wt.% Pb, 55.5wt.% Bi) as primary coolant (the heat generated into the core is further removed by a secondary circuit with water/steam and a tertiary circuit with air).

In subcritical mode, the facility is driven by a high-power proton linear accelerator (linac) delivering a proton beam in CW mode of 600 MeV proton energy and up to 4 mA intensity. The proton beam is driven into the core via a vacuum beam line and impinges on the LBE coolant, which then also acts as spallation target.

In critical mode, the proton beam line is removed and a number of fuel assemblies is added to the core periphery to reach criticality.

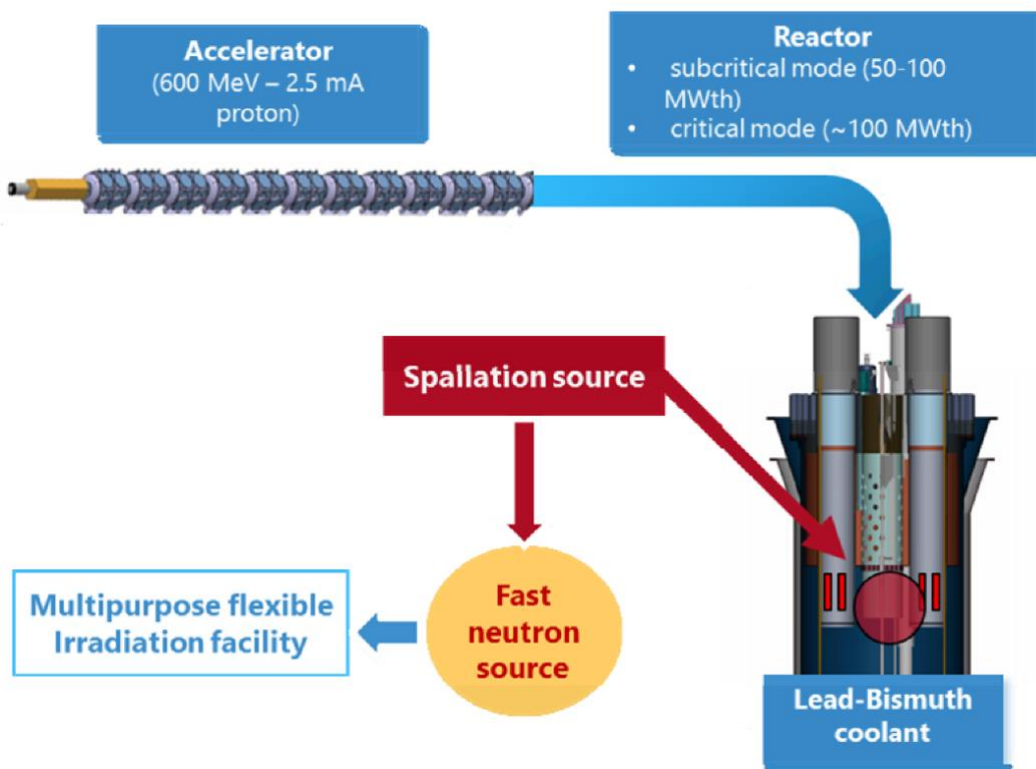


Figure 1.7- The three components of the MYRRHA facility [11]

### 1.5 LBE and LBE conditioning system

Liquid metals have been studied since the early development of fission energy as reactor coolants for fast reactors, fusion energy blanket applications and, more recently, for both accelerator-driven system (ADS) proposed for high-level radioactive waste transmutation

and for generation IV fast reactors. Moreover, heavy liquid metals are being proposed as target materials for high-power neutron spallation sources. [12]

As already mentioned, the MYRRHA design foresees the use of lead-bismuth eutectic both as primary coolant and spallation target material, due to its favourable properties. [13]

The melting point of LBE is about 125°C which is lower than the melting points of each of the individual components (lead 327 °C, bismuth 271 °C). Moreover, LBE is an excellent radiation shield that blocks gamma radiation. Most importantly for ADS applications, LBE has a high neutron yield in spallation reactions with high-energy protons, it has a small neutron absorption cross-section and a small scattering cross-section making it virtually transparent to neutrons.

As a coolant, LBE exhibits high boiling points and high great heat conductivity, which enables the reactor primary system to operate under atmospheric pressure.

During the operation of MYRRHA, impurities will be introduced into the liquid metal by nuclear reactions (activation, spallation) as well as by corrosion processes.

Chemistry control and monitoring is one of the critical issues for the operation of heavy liquid metal nuclear systems. Requirements are placed on contamination by coolant oxides, corrosion and/or dissolution of structural materials. In order to satisfy these requirements, in the MYRRHA design the chemistry control is performed by the LBE Conditioning System (LBECS). One of the main objectives of this system is the control of the oxygen concentration in LBE. An excessive oxygen concentration would in fact lead to formation of solid lead oxide particles in the coolant which, in relevant amounts, represent a safety concern due to subsequent coolant flow blockage risk for the core; a too low oxygen concentration would instead lead to unacceptable corrosion rates of the structural material of the reactor. The LBECS will add or remove oxygen from the coolant as required to maintain its concentration at the desired target values.

### **1.6 Accident scenario**

In the MYRRHA design, the LBE coolant constitutes a source term with very significant radiotoxicity. This is mainly due to the presence of  $^{210}\text{Po}$ , a neutron activation product of  $^{209}\text{Bi}$ . The presence of alpha-active polonium is a great disadvantage of LBE.

During the normal operation of the facility, the LBECS will continuously bring part of the LBE source term out of the reactor barrier: a leak or break of the LBECS may then result in the partial release (spill) of the LBE source term (in liquid form) into the reactor building (Primary Containment).

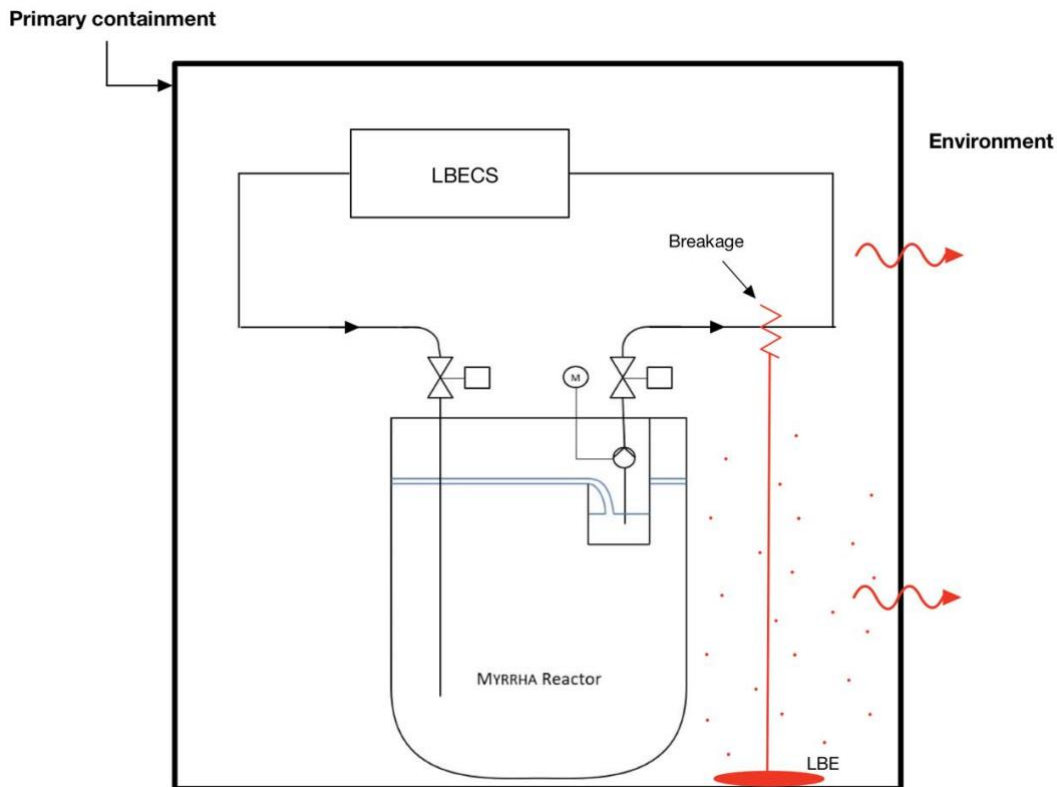


Figure 1.8- Schematic view of the accident scenario

This source term can become airborne due to various processes. A possible source term release mechanism into the Primary Containment atmosphere is LBE aerosol generation by splashing upon impingement of the spilled LBE on solid surfaces (for instance, the floor of the reactor building). This study focuses on the source term component produced by this release mechanism.

### 1.7 Aim of the study

In order to support the safety analysis, this study aims at investigating the LBE in-containment aerosol deposition behavior due to natural processes (i.e. gravitational settling and Brownian motion), by means of the aerosol dynamics models implemented in the MELCOR code.

The interest is placed on the impact that the natural mechanisms of deposition have on the reduction of radioactive material suspended in the containment atmosphere. This reduction will subsequently result in a decrease of the released activity to the environment (via leakages of the Primary Containment barrier) and, eventually, in a decrease of the radiological consequences of the accident.

This study focuses on the dynamic behaviour of the aerosol source term rather than on the radiological consequences caused by its release, which can easily be assessed by

means of existing methodologies, once the evolution of the airborne source term is determined.

Overall, the study aims at acquiring a better understanding of the physical processes in play and at highlighting the most important aspects that characterize the in-containment LBE aerosol depletion behaviour.

---

# Chapter 2

## Modelling approach and tool

---

The aerosol dynamics models implemented in the MELCOR code have been selected to perform this study.

### 2.1 Description of MELCOR core

MELCOR is a computer code developed by Sandia National Laboratories for the U.S. Nuclear Regulatory Commission (NRC). [14] Historically, its primary purpose consisted in the modeling of severe accident progression in Light Water Reactors, therefore many implemented models are specific to the phenomenology of this technology and clearly not applicable to an LBE-cooled fast neutron reactor such as MYRRHA. When it comes to aerosol depletion physics inside the containment, however, the relevant phenomena are largely the same.

MELCOR has a modular structure, composed of a number of different packages, each modelling a different portion of the accident phenomenology. This feature allows the user to select only the packages of interest for the modeling of the physical phenomena at study.

The proposed study solely focuses on the aerosol behaviour in the primary containment environment, therefore, it mainly employs the RadioNuclide (RN) package [14], whose basic approach to aerosol dynamics is described in section 2.2. Other MELCOR packages used for this study are the following ones:

- Material Properties (MP) package, to define the structural materials.
- NonCondensable Gas (NCG) package, to define the containment atmosphere gas.
- Decay Heat (DCH) package, to introduce the aerosol material.
- Control Volume Hydrodynamics (CVH) package, to model the containment structures.
- Executive (EXEC) package, to control the computational parameters.

## 2.2 Aerosol dynamics model implemented in MECOR

The aerosol dynamics model implemented in MELCOR allows to simulate the evolution of the distribution of the considered chemical species with respect to aerosol particle size, by the implementation of a set of balance equations called General Dynamic Equations. The General Dynamic Equations (GDE) are population balance equations governing the time dependence of aerosol concentration in the atmosphere.

MELCOR finds a numerical solution to these equations by introducing a finite sectional approximation of the size domain and by considering aerosol of different chemical species as different components, where a *component* is a particular type of aerosol material and a *section* is one of the size bins in which the size domain is subdivided. [15] Mass conservation is required for each component and section for the processes of agglomeration, particle generation and removal.

The model allows for the definition of the boundaries for the aerosol size domain and the choice of the number of sections in which the size domain is subdivided. This selection comes with limitation on the maximum number of sections acceptable for a defined particle size range.

The maximum number of sections possible in each calculation is given by

$$m = \frac{\log\left(\frac{v_m}{v_0}\right)}{\log(2)} \quad (2.1)$$

Where  $v_0$  and  $v_m$  are the smallest and the largest particle masses in the computational domain, respectively. [16] The masses can be converted into diameters using the assumption of spherical shape.

Given the number of sections and the minimum and maximum aerosol diameter, the individual section boundaries are calculated so that ratio of the upper and lower bound diameter of each section is the same.

This analysis starts with the definition of a single component that describes the LBE aerosol whose behaviour is under investigation.

In this study only natural deposition processes, such as gravitational settling and diffusion by Brownian motion, are considered for agglomeration and removal of suspended aerosol particles inside the containment atmosphere.

### 2.2.1 General Dynamic Equations

It will follow a brief introduction of the formulation of the aerosol balance equation limited to the physical phenomena considered in this proposed modeled scenario. [17]

Starting with the definition of  $Q_l(t)$  as the total mass of aerosol per unit volume of fluid in section  $l$  at time  $t$ .

Thus,

$$Q_l(t) = \sum_{k=1}^s Q_{l,k}(t) = \int_{v_{l-1}}^{v_l} vn(v, t)dv \quad (2.2)$$

where  $Q_{l,k}(t)$  is the mass of component  $k$  in section  $l$ ,  $s$  is the total number of components,  $v_{l-1}$  and  $v_l$  denote the size of the smallest and largest particles, respectively, in section  $l$  and  $n(v, t)$  is the size distribution function. It is noted that  $v_0$  is arbitrary and the upper bound section  $l-1$  is equal to the lower bound of section  $l$  for  $l=2,3, \dots, m$ .

The conservation equations are derived by determining the net rates at which species  $k$  is added to each section by agglomeration and particle source and removal mechanisms.

The rate of coagulation between particles in the mass ranges  $[u, u+du]$  and  $[v, v+dv]$  is given by

$$\beta(u, v)n(u, t)n(v, t) \times dudv \quad (2.3)$$

where  $\beta(u, v) = \beta(v, u)$  is the kinetic agglomeration coefficient.

A function  $\theta$  is introduced in order to add to section  $l$  only particles whose resulting mass is in the range  $[v_{l-1}, v_l]$ . Therefore, the function  $\theta$  will be equal to one only when this condition is satisfied.

The flux of mass into section  $l$  by agglomeration of particles in lower sections may be expressed as

$$\frac{1}{2} \int_{v_0}^{v_{l-1}} \int_{v_0}^{v_{l-1}} \theta(v_{l-1} < (u+v) < v_l)(u+v) \times \beta(u, v)n(u, t)n(v, t)dudv \quad (2.4)$$

It is noted that  $(u+v)$  is included to determine the mass entering section  $l$ .

The flux of mass of component  $k$  into section  $l$  is given by the sum of the masses of component  $k$  in the agglomerating particles. Since particles of the same size may differ in composition, composition may not be a unique function of particle size.

Therefore, it is defined a marginal mass fraction probability density function  $g_k(v, \eta_k)$ , where  $0 \leq \eta_k \leq 1$ , and  $g_k(v, \eta_k)d\eta_k$  is the time-dependent fraction of particles in the mass range  $[v, v+dv]$  with mass fraction of component  $k$  in the range  $[\eta_k, \eta_k + d\eta_k]$ , thus for  $k=1,2,\dots,s$ :

$$\int_0^1 g_k(v, \eta_k)d\eta_k = 1 \quad (2.5)$$

The mean mass of component  $k$  for all particles having mass in the range  $[v, v+dv]$  and  $[u, u+du]$  is defined as

$$\bar{v}_k = \int_0^1 \eta_k g_k(v, \eta_k)d\eta_k \quad (2.6)$$

$$\bar{u}_k = \int_0^1 \xi_k g_k(v, \xi_k)d\xi_k \quad (2.7)$$

Thus, the mass flux of component  $k$  into section  $l$  is given by

$$\frac{1}{2} \int_{v_0}^{v_{l-1}} \int_{v_0}^{v_{l-1}} \theta(v_{l-1} < (u+v) < v_l) \times (\bar{u}_k + \bar{v}_k) \times \beta(u, v)n(u, t)n(v, t)dudv \quad (2.8)$$

Mass is removed from section  $l$  when a particle from section  $l$  agglomerates with a particle from a lower section and forms a particle larger than  $v_l$ . This flux is given by

$$\int_{v_0}^{v_{l-1}} \int_{v_{l-1}}^{v_l} \theta((u+v) > v_l) \bar{u}_k \times \beta(u, v)n(u, t)n(v, t)dudv \quad (2.9)$$

The mass flux of component  $k$  into section  $l$  due to the agglomeration of a particle from a lower section with a particle in section  $l$  and the resulting particle remains in section  $l$ , is given by

$$\int_{v_0}^{v_{l-1}} \int_{v_{l-1}}^{v_l} \theta((u+v) < v_l) \bar{v}_k \times \beta(u, v)n(u, t)n(v, t)dudv \quad (2.10)$$

The next agglomeration term describes the flux of mass of component  $k$  out of section  $l$  due the intrasectional agglomeration if the resulting particle size is greater than  $v_l$  and is given by

$$\frac{1}{2} \int_{v_{l-1}}^{v_l} \int_{v_{l-1}}^{v_l} \theta((u+v) > v_l) (\bar{u}_k + \bar{v}_k) \times \beta(u, v)n(u, t)n(v, t)dudv \quad (2.11)$$

Finally, the mass flux of component  $k$  out of section  $l$  due to agglomeration between a particle within section  $l$  and a particle from a higher section is given by

$$\int_{v_l}^{v_m} \int_{v_{l-1}}^{v_l} \bar{u}_k \beta(u, v) n(u, t) n(v, t) du dv \quad (2.12)$$

To obtain the contribution of the various sections to  $Q_{l,k}$ , the integrals that range over more than one section are replaced by a sum of integral over each section to get the sectional equation for aerosol undergoing only agglomeration:

$$\begin{aligned} \frac{dQ_{l,k}}{dt} = & \frac{1}{2} \sum_{i=1}^{l-1} \sum_{j=1}^{l-1} \int_{v_{i-1}}^{v_i} \int_{v_{j-1}}^{v_j} \theta(v_{l-1} < (u + v) \\ & < v_l) (\bar{u}_k + \bar{v}_k) \beta(u, v) n(u, t) n(v, t) du dv \\ & - \sum_{i=1}^{l-1} \int_{v_{i-1}}^{v_i} \int_{v_{l-1}}^{v_l} \theta((u + v) > v_l) \bar{u}_k \beta(u, v) n(u, t) n(v, t) du dv \\ & + \sum_{i=1}^{l-1} \int_{v_{i-1}}^{v_i} \int_{v_{l-1}}^{v_l} \theta((u + v) < v_l) \bar{u}_k \beta(u, v) n(u, t) n(v, t) du dv \\ & - \frac{1}{2} \int_{v_{i-1}}^{v_i} \int_{v_{l-1}}^{v_l} \theta((u + v) \\ & > v_l) (\bar{u}_k + \bar{v}_k) \beta(u, v) n(u, t) n(v, t) du dv \\ & - \sum_{i=l+1}^m \int_{v_{i-1}}^{v_i} \int_{v_{l-1}}^{v_l} \bar{u}_k \beta(u, v) n(u, t) n(v, t) du dv \end{aligned} \quad (2.13)$$

In order to obtain the sectional equation that describes the aerosol dynamics model employed, mass flows due to source and removal mechanisms have to be introduced.

By assuming only spatially homogeneous sources that are a function of particle size and time. If  $S(v, t)$  is the source rate, the generation rate of component  $k$  in section  $l$  is given by

$$\int_{v_{l-1}}^{v_l} \tilde{v}_k S(v, t) dv \quad (2.14)$$

To account for a source generating particles of the same size but with different compositions,  $\tilde{v}_k$  is used to represent the mean mass of component  $k$  for generated particles of size  $v$ .

The removal of particles can be described as

$$\int_{v_{l-1}}^{v_l} \bar{v}_k R[n(v, t), v, t] dv \quad (2.15)$$

where  $R[n(v, t), v, t]$  is the removal rate of particles in the size range  $[v, v+dv]$ .

In conclusion, the sectional equation for component  $k$  in section  $l$  is expressed as

$$\begin{aligned} \frac{dQ_{l,k}}{dt} = & \frac{1}{2} \sum_{i=1}^{l-1} \sum_{j=1}^{l-1} \int_{v_{i-1}}^{v_i} \int_{v_{j-1}}^{v_j} \theta(v_{l-1} < (u+v) \\ & < v_l) (\bar{u}_k + \bar{v}_k) \beta(u, v) n(u, t) n(v, t) dudv \\ & - \sum_{i=1}^{l-1} \int_{v_{i-1}}^{v_i} \int_{v_{l-1}}^{v_l} \theta((u+v) > v_l) \bar{u}_k \beta(u, v) n(u, t) n(v, t) dudv \\ & + \sum_{i=1}^{l-1} \int_{v_{i-1}}^{v_i} \int_{v_{l-1}}^{v_l} \theta((u+v) < v_l) \bar{u}_k \beta(u, v) n(u, t) n(v, t) dudv \\ & - \frac{1}{2} \int_{v_{i-1}}^{v_i} \int_{v_{l-1}}^{v_l} \theta((u+v) \\ & > v_l) (\bar{u}_k + \bar{v}_k) \beta(u, v) n(u, t) n(v, t) dudv \\ & - \sum_{i=l+1}^m \int_{v_{i-1}}^{v_i} \int_{v_{l-1}}^{v_l} \bar{u}_k \beta(u, v) n(u, t) n(v, t) dudv \\ & + \int_{v_{l-1}}^{v_l} \bar{v}_k S(v, t) dv - \int_{v_{l-1}}^{v_l} \check{v}_k R[n(v, t), v, t] dv \end{aligned} \quad (2.16)$$

To better comprehend the influence that the processes of diffusion by Brownian motion and of gravitational settling have on the equation governing the aerosol dynamics model, a few considerations are dedicated to the functional dependence of the agglomeration coefficient and to the definition of the removal rate in the following sections.

### 2.2.1.1 Agglomeration coefficient

The value of the agglomeration coefficient  $\beta$  depends upon the aerosol and atmosphere properties. In the previous equations, the dependence of the agglomeration coefficient is placed on the values of the agglomeration of particle masses ( $\beta(u, v)$ ). Its dependence can be also expressed on the particle size since the code converts the mass to radius using the assumption of spherical shape with a set value of density.

The dependence on atmosphere properties is not considered to be a major source of uncertainty in the aerosol calculations. [15] The MELCOR code derives the total value of the agglomeration coefficient as the sum of kernels, each of which is related to a different physical process. The agglomeration processes considered in this aerosol system

are diffusion by Brownian motion and gravitational settling. The dependence on particle diameter and key modeling parameters of the components related to the two deposition processes is presented, respectively, in equation 2.17 and 2.18. [15]

$$\beta_B \propto \gamma \chi^{-1} f(d_i, d_j) \quad (2.17)$$

$$\beta_{grav} \propto \varepsilon_g \gamma^2 \chi^{-1} (d_i + d_j)^2 (d_i^2 - d_j^2) \quad (2.18)$$

In these proportionalities,  $\gamma$  and  $\chi$  are the agglomeration and dynamic shape factors, respectively. The gravitational collision efficiency is represented by  $\varepsilon_g$  and assumes a specific value calculated in the code. A description of these aerosol parameters will be given in the following section (section 2.2.2). Variables  $d_i$  and  $d_j$  are the diameters of the two interacting particles, with  $d_i > d_j$ . The magnitude of the Brownian kernel increases with increasing values of the size ratio  $d_i / d_j$ .

#### 2.2.1.2 Removal of particles

In the aerosol system modeled, the removal of particles from the atmosphere is due to the processes of the diffusion by Brownian motion and gravitational settling. The physics of these two processes is addressed in the equation 2.16 by term including the removal rate. The kernels of the removal rate in equation 2.15 for gravitational settling and deposition by Brownian diffusion are, respectively, given by

$$R_{grav} = \frac{A_{floor}}{V_c} \cdot v_{grav} \quad (2.19)$$

$$R_{diff} = \frac{A_{diff}}{V_c} \cdot v_{diff} \quad (2.20)$$

where  $A_{floor}$  is the floor surface,  $A_{diff}$  is the total surface available for diffusion by Brownian motion,  $V_c$  is the total volume of the chamber and  $v_{grav}$  and  $v_{diff}$  are, respectively, the gravitational deposition velocity and the diffusive deposition velocity.

The deposition velocities due to the two mechanical processes of gravitational settling and deposition by Brownian motion, respectively, given by

$$v_{grav} = \frac{d_p^2 \rho_p g C_m}{18 \mu \chi} \quad (2.21)$$

$$v_{diff} = \frac{\sigma T C_m}{3\pi \mu \chi d_p \delta_D} \quad (2.22)$$

where

$d_p$  the particle diameter

$\rho_p$  is the particle density

$g$  is the acceleration of gravity (9.8 m/s<sup>2</sup>)

$C_m$  is the Cunningham slip correction factor, defined in section 2.2.2

$\mu$  is the viscosity of the atmospheric gas

$\chi$  is the dynamic shape factor, defined in section 2.2.2

$\sigma$  is the Boltzmann constant (1.38 · 10<sup>-23</sup> J/K<sup>-1</sup>)

$T$  is the atmosphere temperature

$\delta_D$  is the diffusion boundary layer thickness, defined in section 2.2.2

### 2.2.2 Main parameters characterizing aerosol physics

Aerosol particles not usually assumed to be spherical and the effective aerosol densities may be significantly less than the bulk density of the material of which the aerosol is composed. In aerosols codes, these effects may be taken into account by using a formalism based on fully dense spherical aerosols modified through the use of the agglomeration shape factor  $\gamma$  and the dynamic shape factor  $\chi$ . [15] Their values are input into the code by the user.

The dynamic shape factor is used to correct the equations describing Stoke's law to take into consideration the departure from idealized conditions in which the particles are considered spherical.

Stoke's law describes the resistance or drag force ( $F_D$ ) of a particle moving through a fluid and it can be expressed as:

$$F_D = 3\pi\eta Vd \quad (2.23)$$

where  $\eta$  is the viscosity of the fluid,  $V$  and  $d$  are, respectively, the velocity and the diameter of the particle.

The dynamic shape factor is defined as the ratio of the actual resistance force of the nonspherical particle to the resistance force of a sphere having the same volume and velocity.

The dynamic shape factor is given by

$$\chi = \frac{F_D}{3\pi\eta V d_e} \quad (2.24)$$

where  $d_e$  is the equivalent volume diameter, which is the diameter of the sphere having the same volume as the irregular particle.

For nonspherical particles the value of the dynamic shape factor differs from the unity.

The gravitational collision efficiency is represented by  $\varepsilon_g$  and it depends on the hydrodynamic interactions between two particles. The hydrodynamic interaction between two particles is the tendency of a particle to follow streamlines in flowing around another particle and it leads to a collision cross section that is smaller than the geometric cross section. If there was no hydrodynamic interaction between two particles, the larger particle will pick up all smaller particles as it falls, and the gravitational efficiency would be a constant equal to one. This does not happen because smaller particles tend to be pushed out of the way by the flow of gas around the larger ones. In MELCOR the value of the gravitational collision efficiency is given by

$$\varepsilon_g = 1.5 \left( \frac{d_j}{d_i + d_j} \right)^2 \quad (2.25)$$

Aerosol particles in can be small enough that the motion of these particles cannot be deduced by treating the gas phase as a continuum. The Cunningham slip correction factor is introduced to account for non-continuum effects.

The Cunningham slip correction factor [18] is given the equation:

$$C_m = 1 + \frac{2\lambda}{d_p} [F_{slip} + 0.4 \exp(-1.1d_p/2\lambda)] \quad (2.26)$$

In formula,  $F_{slip}$  is the slip factor and  $\lambda$  is the mean free path of the atmospheric gas.

The value of the slip correction factor is given by

$$F_{slip} = \frac{2\mu}{\lambda\rho_g c_m} \quad (2.27)$$

where  $\rho_g$  is the gas density and  $c_m$  is the mean velocity of the gas molecule.

The mean velocity of the gas molecule is calculated as

$$c_m = \left( \frac{8RT}{\pi M_w} \right)^{1/2} \quad (2.28)$$

where  $R$  is the universal gas constant and  $M_w$  is the gas molecular weight.

Additionally, MELCOR requires the input of the value of the sticking coefficient. The sticking coefficient indicates the probability that when particles come into contact, they would stick together. Its value could vary from 0 to 1. A sticking coefficient lower than 1 would indicate that not all particles coming into contact will remain in contact.

Diffusion layer boundary thickness is a thin layer of fluid at the interface with a solid surface in which frictional forces causes the diffusion process to become the dominant mode of deposition.

The MELCOR code assumes that the aerosol particles are uniformly mixed in the containment atmosphere, with the exception of the diffusional boundary layer at the wall where aerosol deposition takes place. Its value is user defined.

### 2.2.3 Assumptions and approximations

The MELCOR modeling approach introduces certain approximations and implements certain assumptions. [15] The assumptions and approximations that are most relevant for this study will be briefly discussed:

- The aerosol particle number density within a control volume has no spatial dependence. Therefore, the aerosol particles are always assumed to be homogeneously distributed.
- The distribution of aerosol mass within a section is treated as constant with respect to the logarithm of particle mass.
- All aerosol particles that are calculated to grow larger than the maximum section size defined by the user are assumed to instantaneously fallout onto either horizontal surfaces or onto adjacent lower control volumes. In this study, a single cell approach is used to model the control volume, therefore all particles that fall out will deposit directly onto the horizontal surface.
- Whenever two or more physical processes occur simultaneously, it is assumed that each one acts independently. In this study, the two natural deposition processes that drive the dynamic evolution of the aerosol population affect particles in different size ranges. Generally, deposition by Brownian motion is significant for particles below 0.1  $\mu\text{m}$  whereas gravitational settling dominates for particles above that size. Therefore, the additivity of the effects of these two phenomena can be regarded as a good approximation.

- All aerosol components have the same density. In the proposed study, the density of LBE ( $10000 \text{ kg/m}^3$ ) is used. This code limit prevents from simulating the presence of structural aerosols (which would have a much lower density) in the containment atmosphere before accident onset (which is a conservative approximation, as it would lead to increased agglomeration and faster deposition of the radioactive LBE aerosols).

### 2.3 Primary containment model

The primary containment in this study is modeled in MELCOR as a single control volume of rectangular section. The volume ( $52371 \text{ m}^3$ ) is filled by Nitrogen gas, consistently with the design of the MYRRHA facility, which foresees a dry inert nitrogen atmosphere inside the reactor hall. The temperature of the containment atmosphere is set to the constant value of  $40^\circ\text{C}$  and the pressure of the Nitrogen gas is set to 1 atm.

The boundary conditions of the containment structure are set to be adiabatic.

No flow is considered in this model, therefore, excluding every form of turbulent phenomena, only leaving gravitation and diffusion by Brownian motion as agglomeration and deposition mechanisms.

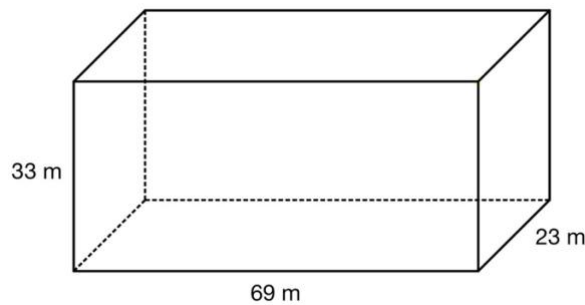


*Figure 2.1- Control volume*

---

# Chapter 3

## Sensitivity analysis with monodisperse aerosol source

---

### 3.1 Objective of the analysis

The simulations of the modeled system, performed in this initial phase of the analysis, are aimed at studying the influence of initial aerosol size and aerosol mass released on the evolution of the suspended aerosol mass in the Primary Containment.

The results obtained are going to be analyzed to get a better understanding of the physical behaviour of the aerosol particles population. The knowledge derived will give useful indications for further analysis of the system under investigation.

### 3.2 Methodological approach

The Primary Containment model introduced in the previous chapter in section 2.3 is used for all MELCOR simulations presented in this part of the study.

Section	Boundaries
1	1-1.58 nm
2	1.58-2.51 nm
3	2.51-3.98 nm
4	3.98-6.31 nm
5	6.31-10.0 nm
6	10.0-15.8 nm
7	15.8-25.1 nm
8	25.1-39.8 nm
9	39.8-63.1 nm
10	63.1-100 nm
11	100-158 nm
12	158-251 nm
13	251-398 nm
14	398-631 nm
15	0.631-1.0 $\mu\text{m}$
16	1.0-1.58 $\mu\text{m}$
17	1.58-2.51 $\mu\text{m}$
18	2.51-3.98 $\mu\text{m}$
19	3.98-6.31 $\mu\text{m}$
20	6.31-10.0 $\mu\text{m}$

As a first step, the lower and upper limits of the size range of the aerosol particles are set, respectively, to 0.001  $\mu\text{m}$  and 10  $\mu\text{m}$ , covering a wide range of possible aerosol particle sizes. The size range, as requested by the aerosol dynamics model implemented, is divided into sections. The number of sections chosen to discretize the particle size domain is 20. Table 3.1 reports the values of the particle diameters that are the boundaries of each section. The values of general parameters characterizing the aerosol, some of which will be the interest of a more in-depth investigation in the upcoming chapter, are presented in section 3.2.1. The sensitivity analysis is made with regard to the quantity of aerosol mass released and to the size of the particles introduced into the system.

For the LBE mass inventory released in aerosol form, three different values of 10 kg, 100 kg and 1000 kg are chosen in order to observe the response of the system at different initial concentrations.

Table 3.1- Sections and respective boundary diameters

For each of these values, several simulations are performed where the total mass inventory is instantaneously released at the onset of each considered transient into each of the 20 sections.

The transient duration is initially set to one month. Changes to this value are considered in subsequent runs, as explained in section 3.3.1 to optimize the computational cost.

#### **3.2.1 Values of the aerosol input parameters**

The main parameters characterizing the aerosol physics have been introduced in the previous chapter in section 2.2.2. In order to perform the sensitivity analysis, values for each of the parameters that require a user defined input value have to be set.

For the dynamic shape factor a value of 5 is selected to account for the departure from ideal spherical condition. This choice is derived from the dependencies for the agglomeration coefficients given in equation 2.17 and 2.18 and deposition velocities (equations 2.21 and 2.22), showing that a high value of the dynamic shape factor is conservative, as it leads to slower aerosol agglomeration and deposition. A literature review highlighted a reasonable variation range for this parameter between 1 and 5, as it will be further discussed in section 4.2.2.3.

Following the same reasoning, the agglomeration shape factor is left to the default value of one, since the unit value is the most conservative value that this parameter could assume, in terms of agglomeration rate and deposition velocity.

There is no reason to believe that two particles of LBE aerosol would not stick together once they come in contact. Therefore, the sticking coefficient is left to the default value of one.

The required value for the slip factor, in order to allow the calculation of the Cunningham slip correction factor by the code, is calculated for the aerosol material (LBE) and atmosphere gas (Nitrogen) under investigation according to equation 2.27. The resulting value is 0.697.

### **3.3 Results**

The main parameter of interest in the obtained results is the suspended mass of aerosol in the containment atmosphere, since it is directly related to the source term released to the environment in case of containment leakage, which determines the radiological consequences of the accident at study.

In order to better understand some of the results obtained, a closer look at the evolution of the size of aerosol particles is taken.

Furthermore, the mass deposited on the physical boundaries of the control volume, defined within the code as heat structures, is analyzed to assess the impact of each of the two considered natural deposition processes (gravitational settling and diffusion by Brownian motion) on the overall deposited mass and better understand the physical behaviour of the system.

### 3.3.1 Influence of initial aerosol size

The first results consider the release of 100 kg in each of the sections.

The table below shows the suspended mass after one week and after one month from the initial aerosol release in each of the 20 sections.

Size bin in which initial mass is released	Suspended mass at the end of the transient (kg)	
	1 week	1 month
1-1.58 nm	2.50E+00	2.31E-02
1.58-2.51 nm	2.50E+00	2.31E-02
2.51-3.98 nm	2.50E+00	2.31E-02
3.98-6.31 nm	2.50E+00	2.31E-02
6.31-10.0 nm	2.50E+00	2.31E-02
10.0-15.8 nm	2.50E+00	2.31E-02
15.8-25.1 nm	2.50E+00	2.31E-02
25.1-39.8 nm	2.50E+00	2.31E-02
39.8-63.1 nm	2.50E+00	2.31E-02
63.1-100 nm	2.50E+00	2.31E-02
100-158 nm	2.50E+00	2.30E-02
158-251 nm	2.50E+00	2.30E-02
251-398 nm	2.50E+00	2.30E-02
398-631 nm	2.48E+00	2.28E-02
0.631-1.0 µm	2.37E+00	1.88E-02
1.0-1.58 µm	1.64E+00	1.25E-03
1.58-2.51 µm	2.02E-01	1.06E-08
2.51-3.98 µm	1.77E-04	1.86E-22
3.98-6.31 µm	1.66E-12	0.00E+00
6.31-10.0 µm	8.73E-33	0.00E+00

Table 3.2 - Suspended mass after one week and one month for the release in each size bin

The most striking outcome is that the airborne mass at the end of the transient does not show noticeable variations for large range of initial particle sizes (from 1 nm up to about 1 µm).

Even considering the most conservative result obtained, the mass of suspended aerosol in the containment atmosphere after a month is less than 0.02% of the initial mass released. Figure 3.1 allows to better visualize the evolution of the suspended mass during the transient and observe the steep decrease of its value.

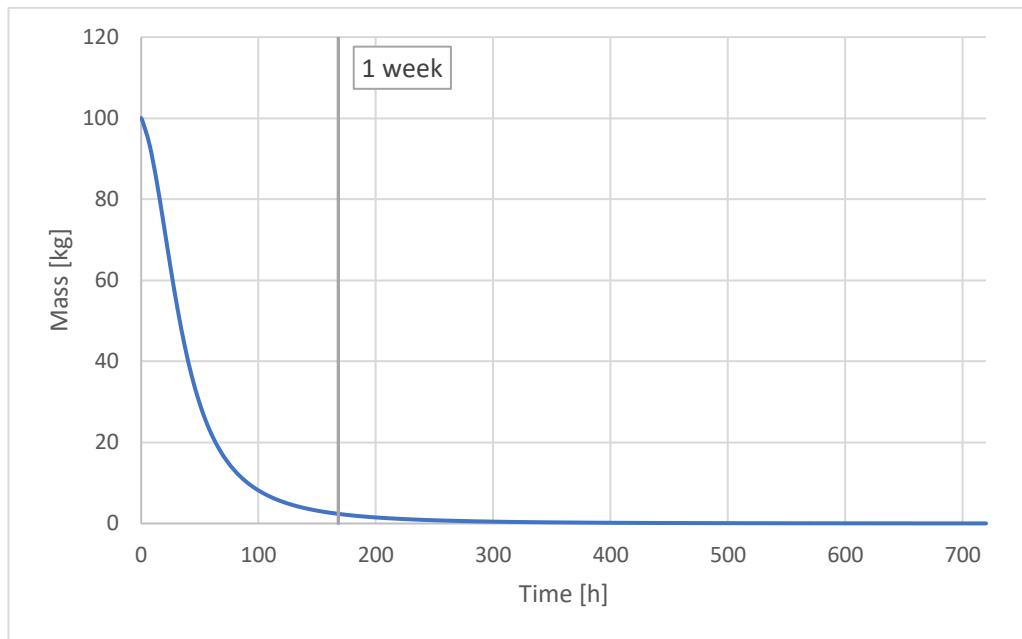


Figure 3.1- Mass suspended when 100 kg of aerosol mass are released in the range 0.631-1.0  $\mu\text{m}$

The observed evolution suggests concentrating further computational effort on a shorter timescale. The total transient duration is set to 1 week for all subsequent studies.

In order to better comprehend the lack of variation in the suspended mass when different sizes of particles are released, the evolution of the particle size distribution can be analyzed. To do so, the value of the parameter Mass Median Diameter (MMD) of the suspended mass during the transient is considered. The mass median diameter is the diameter for which half of the mass is contributed by particles larger than MMD and half by particles smaller than the MMD. [15]

The two competing mechanisms are agglomeration and deposition.

When the particles are released into a sub-micron section, a significant increase in value of the MMD of the airborne aerosol is observed during the first phase of the transient (within 48 hours from release onset): agglomeration is therefore the dominating mechanism. The subsequent decrease in MMD value can be attributed to the more rapid deposition of particles of larger sizes.

The two figures below show the evolution of the value of the MMD in case the release of the total mass inventory occurs in the first section (Figure 3.2) and in the section that has as upper boundary the diameter of 1.0  $\mu\text{m}$  (Figure 3.3). Except for the very first instants of the transient, they both display an almost superimposable progression of the value, with the same peak value.

it can be observed that, for a 100 kg release of sub-micron particles, a very fast agglomeration characterizes the first phase of the transient, causing a sharp increase in the values of the MMD. Hence, whenever the aerosol particles are released in a size bin below the 1  $\mu\text{m}$  value, their MMD quickly converges to the same values, independently of the selected size bin. This fast agglomeration is the reason why, for a wide range of initial particle diameter, the transient behavior (which is determined by the MMD) is substantially the same.

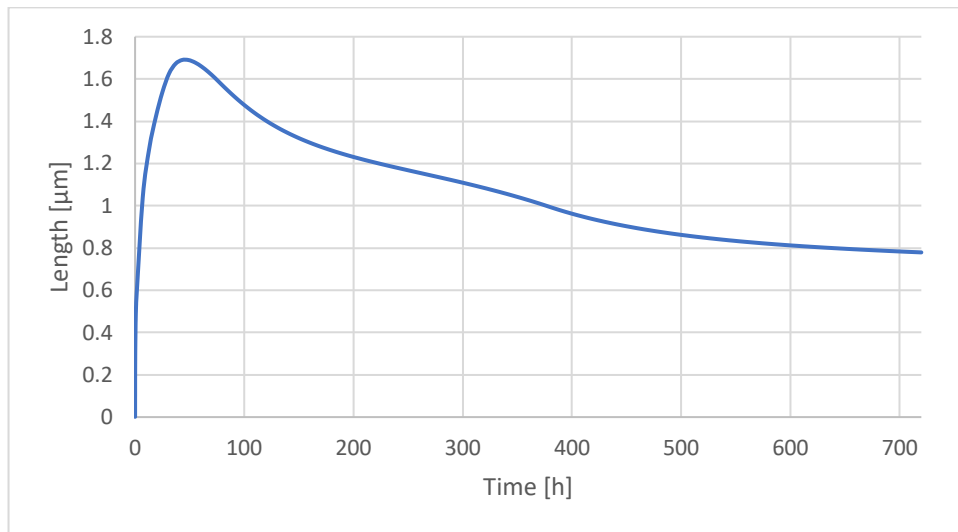


Figure 3.2- Evolution of the value for MMD when the mass is released in the range 1.0-1.58 nm

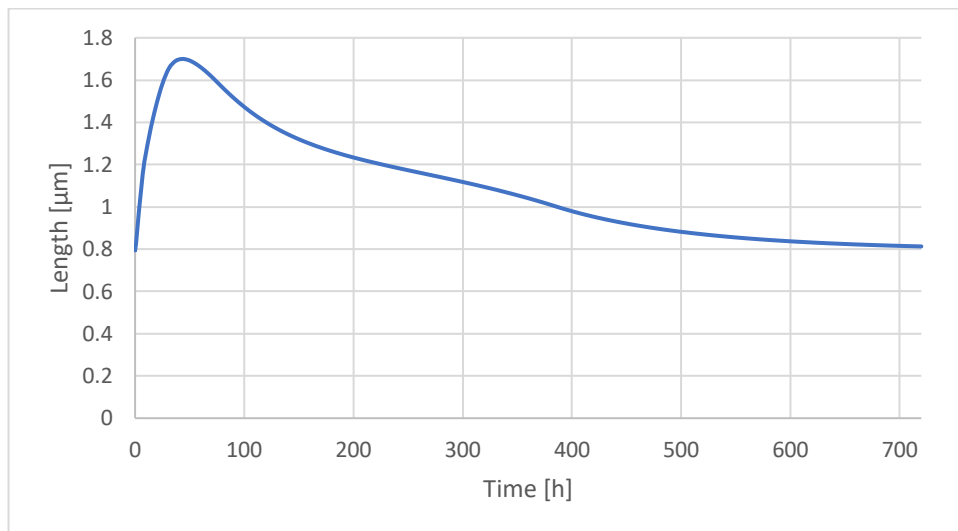


Figure 3.3- Evolution of the value for MMD when the mass is released in the range 0.631-1.0  $\mu\text{m}$

When the particles are released into a large-size section (with diameter above 1  $\mu\text{m}$ ), the behaviour of the MMD differs from the one described above and this is reflected in the values of suspended mass, as it can be observed in Table 3.2 and Figure 3.5.

Figure 3.4 shows that the increase of the MMD is less significant (almost non-existent) if compared with the release in sub-micron sections and limited to the first few hours of the transient. This behaviour means that the process of deposition quickly prevails over the agglomeration. It is justified by the fast deposition velocity of the particles due to their substantial initial size.

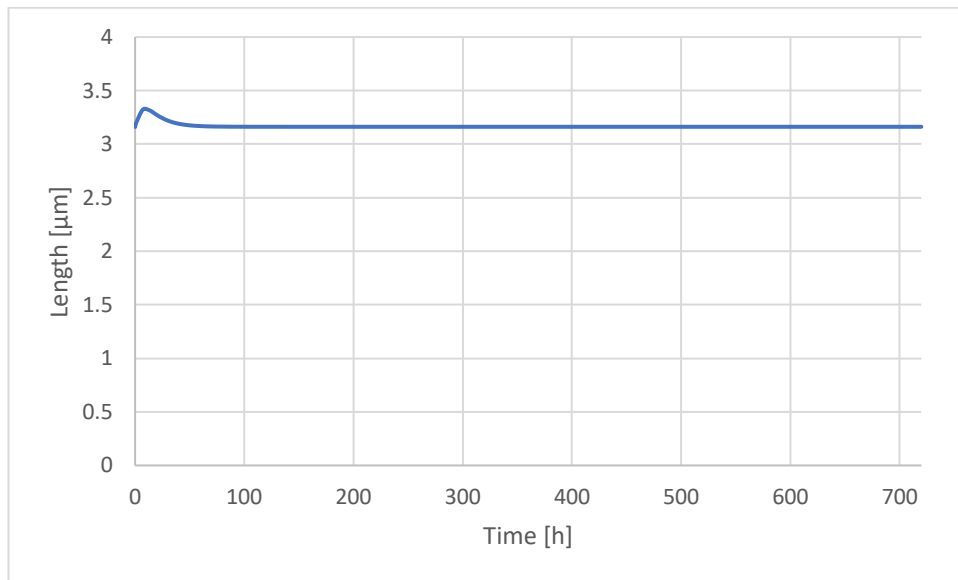


Figure 3.4- Evolution of the value for MMD when the mass is released in the range 2.51-3.98  $\mu\text{m}$

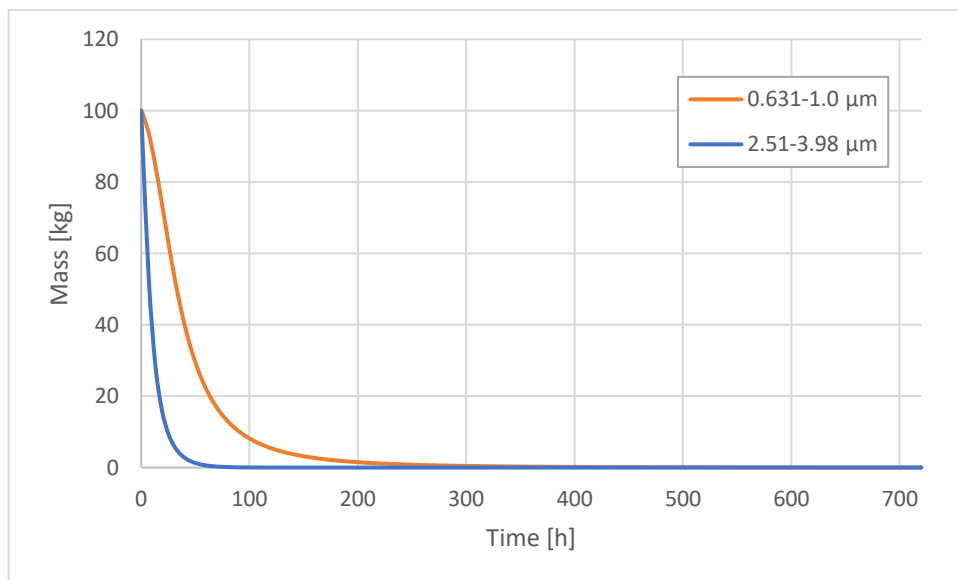


Figure 3.5- Comparison of the mass suspended when 100 kg of aerosol mass are released in the range 0.631-1.0  $\mu\text{m}$  and 2.51-3.98  $\mu\text{m}$

### 3.3.2 Influence of initial aerosol mass

To study the influence of the initial aerosol mass, the computational effort is focused on a one-week transient: as already mentioned in the previous section, the majority of the deposition occurs in this phase.

The results for the suspended mass are given in Table 3.3 a few hours, one day and one week after the onset of the transient (i.e. after the instantaneous release of the aerosol source). In addition to the release of 100 kg, releases of 10 kg and 1000 kg are also considered. Their influence on the suspended mass can also be seen in Figure 3.4.

Size bin in which initial mass is released	Suspended mass after 6.75h (kg)			Suspended mass after 24h (kg)			Suspended mass after 1 week (kg)		
	1000 kg released	100 kg released	10 kg released	1000 kg released	100 kg released	10 kg released	1000 kg released	100 kg released	10 kg released
1-1.58 nm	513.45	95.75	9.89	67.89	68.66	9.24	1.62	2.50	2.62
1.58-2.51 nm	513.45	95.75	9.89	67.89	68.66	9.24	1.62	2.50	2.62
2.51-3.98 nm	513.45	95.75	9.89	67.89	68.66	9.24	1.62	2.50	2.62
3.98-6.31 nm	513.45	95.75	9.89	67.89	68.66	9.24	1.62	2.50	2.62
6.31-10.0 nm	513.45	95.75	9.89	67.89	68.66	9.24	1.62	2.50	2.62
10.0-15.8 nm	513.45	95.75	9.89	67.89	68.66	9.24	1.62	2.50	2.62
15.8-25.1 nm	513.45	95.75	9.89	67.89	68.66	9.24	1.62	2.50	2.62
25.1-39.8 nm	513.45	95.75	9.89	67.89	68.66	9.24	1.62	2.50	2.62
39.8-63.1 nm	513.44	95.75	9.89	67.89	68.66	9.24	1.62	2.50	2.62
63.1-100 nm	513.44	95.75	9.89	67.89	68.66	9.24	1.62	2.50	2.62
100-158 nm	513.42	95.74	9.89	67.89	68.65	9.24	1.62	2.50	2.62
158-251 nm	513.28	95.73	9.89	67.88	68.63	9.23	1.62	2.50	2.62
251-398 nm	512.55	95.66	9.87	67.85	68.50	9.20	1.62	2.50	2.60
398-631 nm	508.86	95.31	9.81	67.67	67.86	9.05	1.62	2.48	2.51
0.631-1.0 µm	491.23	93.92	9.63	66.55	64.98	8.54	1.59	2.37	2.06
1.0-1.58 µm	423.65	89.51	9.17	59.18	54.94	7.23	1.17	1.64	0.89
1.58-2.51 µm	280.33	77.91	8.12	36.23	33.33	4.67	0.16	0.20	0.05
2.51-3.98 µm	138.39	54.09	5.97	11.67	10.39	1.58	0.00	0.00	0.00
3.98-6.31 µm	53.45	23.00	2.78	1.17	0.76	0.11	0.00	0.00	0.00
6.31-10.0 µm	11.92	3.42	0.42	0.00	0.00	0.00	0.00	0.00	0.00

Table 3.3.- Suspended mass at different time steps with different quantities of mass released

It can be highlighted that:

- At the end of a one-week transient, there is almost no difference in the suspended aerosol mass for releases in the range 10-1000 kg.
- for the release of 1000 kg and 100 kg, the suspended mass At the end of a 24-hour transient has comparable values for every size range, whereas the release of 10 kg results into considerably lower values. For each of the quantities released, no difference is observed in the suspended mass for releases in the range 0.001-1 µm, consistently with the results presented in section....
- At the end of a 6.75-hour transient, different values for the suspended mass are observed when different masses are released at transient onset. Still, no difference is still observed in the suspended mass for releases in the range 0.001-1 µm.

The lack of variation in the evolution of the suspended mass for initial particle sizes in the sub-micron range is observed for every considered value of initial mass released. As

explained above, this is due to the rapid agglomeration process at the beginning of these transients.

It is interesting to notice that, as shown in Figure 3.6, a lower release of aerosol mass at transient onset does not directly translate into a reduction of the suspended mass present at the end of the transient.

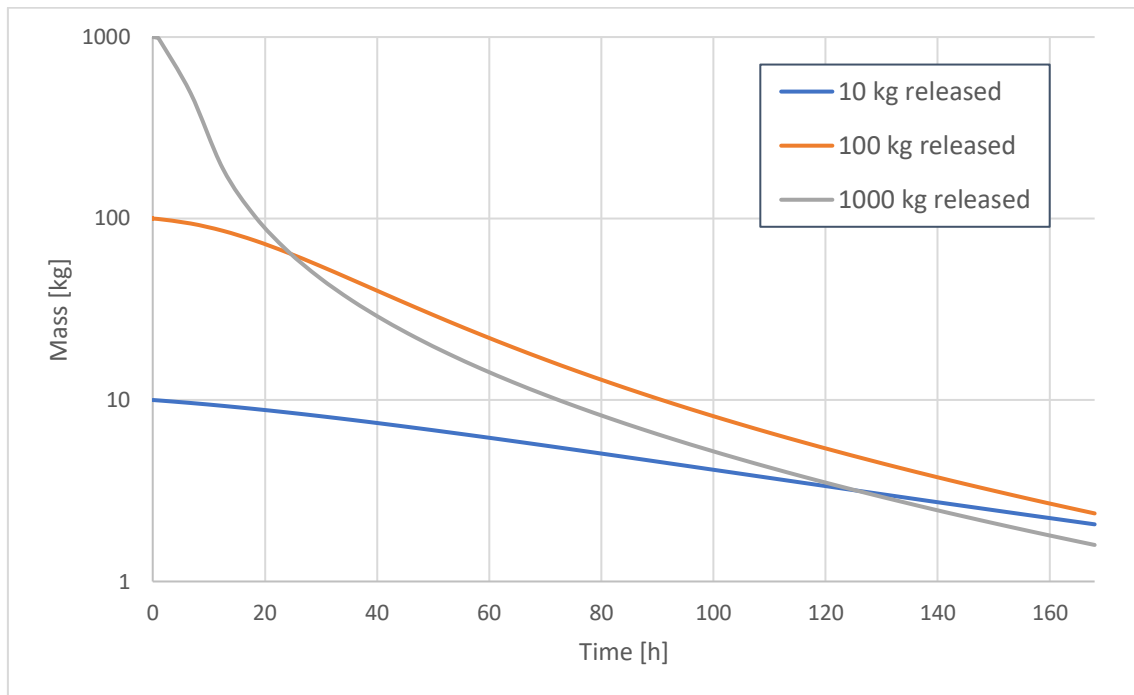


Figure 3.6- Mass suspended when different amounts of aerosol mass are released in the range  $0.631-1.0 \mu\text{m}$  (logarithmic mass scale)

The evolution of the values of the MMD for the different values of initial aerosol mass released is compared in Figure 3.7.

At lower aerosol concentrations, the increase of the value of MMD is less sharp due to slower agglomeration. The faster agglomeration, that is observed to be characteristic of higher concentration releases, generates higher peak values earlier into the transient. This is the expected behaviour of the aerosol system, which is described by the GDE. The direct correlation between the agglomeration rate and the particle concentration was shown in equation 2.3. The maximum value of MMD is the result of the competing processes of agglomeration and deposition, thus, it is clear that if the agglomeration process is slower it will feel more the competition of the deposition mechanisms.

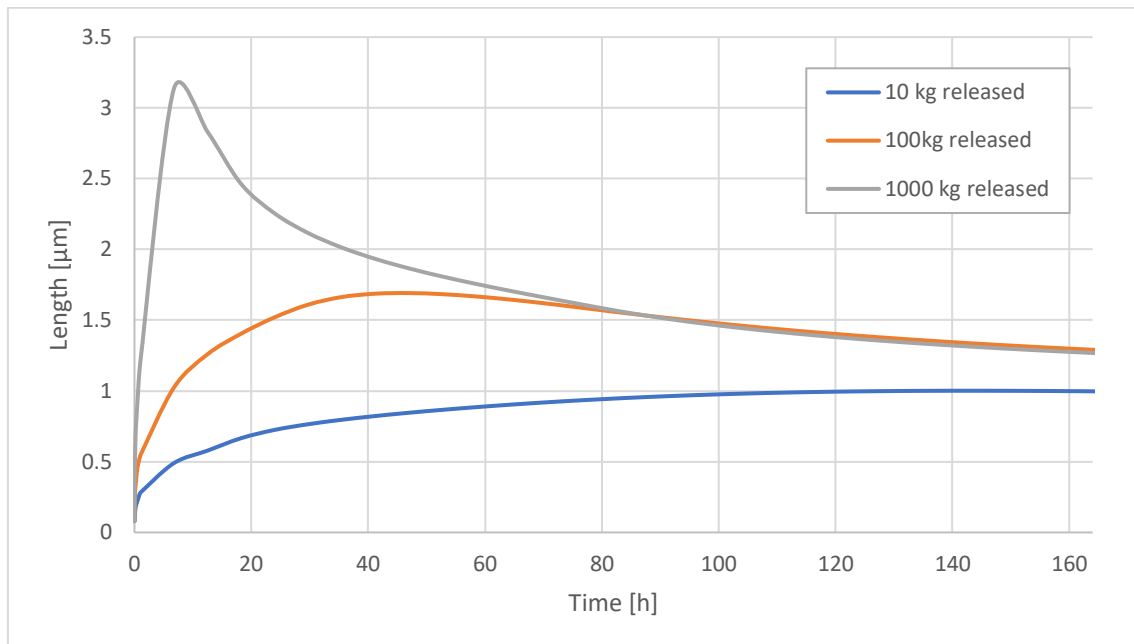


Figure 3.7- Evolution of the values for MMD when different values of aerosol mass are released in the range 63.1-100 nm

### 3.3.3 Deposition on heat structures

The deposition of the aerosol mass on heat structures is due to two natural deposition mechanism: gravitational settling and diffusion due to Brownian motion.

The Table 3.4 reports the mass deposited onto walls (all vertical surfaces that delimit the control volume), ceiling and floor after a one-week transient.

The deposition onto walls and ceiling is exclusively due to Brownian diffusion and, even for initial release of small particles, it gives a negligible contribution to the overall quantity of deposited mass.

Floor deposition is due both to gravitational settling and Brownian diffusion.

It can be concluded that aerosol deposition in the proposed model is mainly driven by the physical mechanism of gravitational settling in the whole aerosol size range considered.

Another artificial deposition mechanism that is introduced by the aerosol dynamics model implemented in MELCOR is the fall out. The fall out consists in the instantaneous deposition of all particles that grow larger than an upper limit value for the particle diameter set by the user. The fall out does not model a physical process, but it is a result of an assumption of the model.

Fall out contributes to a substantial part of the deposition (in this analysis up to about 50%) when high concentrations of aerosol material are released in the sections towards the end of the size range. At low concentrations its contribution is lower and mostly limited at the release in the very last section of the size domain.

In order to verify the influence of the fall out on the deposition, additional simulations are performed with an increased value of the upper limit for the diameters bringing it up to 100  $\mu\text{m}$ .

By doing so, it is observed that the fraction of deposited mass related to fall out is drastically reduced even for releases in the last section of the size range. Therefore, the expansion of the size domain considered allow for a limited influence of the fall out deposition process on the results.

Size bin in which initial mass is released	Deposited mass after 1 week (kg)								
	1000 kg released			100 kg released			10 kg released		
	Walls	Ceiling	Floor	Walls	Ceiling	Floor	Walls	Ceiling	Floor
1-1.58 nm	1.26E-02	2.04E-06	9.98E+02	7.98E-03	2.04E-06	9.75E+01	3.13E-03	2.04E-06	7.37E+00
1.58-2.51 nm	1.26E-02	1.97E-06	9.98E+02	7.98E-03	1.97E-06	9.75E+01	3.13E-03	1.97E-06	7.37E+00
2.51-3.98 nm	1.26E-02	1.88E-06	9.98E+02	7.98E-03	1.88E-06	9.75E+01	3.13E-03	1.88E-06	7.37E+00
3.98-6.31 nm	1.26E-02	1.77E-06	9.98E+02	7.98E-03	1.77E-06	9.75E+01	3.13E-03	1.77E-06	7.37E+00
6.31-10.0 nm	1.26E-02	1.63E-06	9.98E+02	7.98E-03	1.63E-06	9.75E+01	3.13E-03	1.63E-06	7.37E+00
10.0-15.8 nm	1.26E-02	1.44E-06	9.98E+02	7.98E-03	1.44E-06	9.75E+01	3.13E-03	1.44E-06	7.37E+00
15.8-25.1 nm	1.26E-02	1.14E-06	9.98E+02	7.98E-03	1.14E-06	9.75E+01	3.13E-03	1.14E-06	7.37E+00
25.1-39.8 nm	1.26E-02	6.47E-07	9.98E+02	7.97E-03	6.47E-07	9.75E+01	3.13E-03	6.47E-07	7.37E+00
39.8-63.1 nm	1.26E-02	0.00E+00	9.98E+02	7.97E-03	0.00E+00	9.75E+01	3.12E-03	0.00E+00	7.37E+00
63.1-100 nm	1.26E-02	0.00E+00	9.98E+02	7.96E-03	0.00E+00	9.75E+01	3.11E-03	0.00E+00	7.37E+00
100-158 nm	1.26E-02	0.00E+00	9.98E+02	7.94E-03	0.00E+00	9.75E+01	3.09E-03	0.00E+00	7.37E+00
158-251 nm	1.25E-02	0.00E+00	9.98E+02	7.89E-03	0.00E+00	9.75E+01	3.04E-03	0.00E+00	7.38E+00
251-398 nm	1.24E-02	0.00E+00	9.98E+02	7.76E-03	0.00E+00	9.75E+01	2.92E-03	0.00E+00	7.40E+00
398-631 nm	1.21E-02	0.00E+00	9.98E+02	7.44E-03	0.00E+00	9.75E+01	2.62E-03	0.00E+00	7.49E+00
0.631-1.0 $\mu\text{m}$	1.12E-02	0.00E+00	9.98E+02	6.62E-03	0.00E+00	9.76E+01	1.96E-03	0.00E+00	7.93E+00
1.0-1.58 $\mu\text{m}$	8.84E-03	0.00E+00	9.99E+02	4.67E-03	0.00E+00	9.84E+01	9.77E-04	0.00E+00	9.11E+00
1.58-2.51 $\mu\text{m}$	4.80E-03	0.00E+00	1.00E+03	2.06E-03	0.00E+00	9.98E+01	3.06E-04	0.00E+00	9.95E+00
2.51-3.98 $\mu\text{m}$	1.93E-03	0.00E+00	1.00E+03	6.31E-04	0.00E+00	1.00E+02	7.93E-05	0.00E+00	1.00E+01
3.98-6.31 $\mu\text{m}$	7.21E-04	0.00E+00	1.00E+03	1.74E-04	0.00E+00	1.00E+02	2.01E-05	0.00E+00	1.00E+01
6.31-10.0 $\mu\text{m}$	2.47E-04	0.00E+00	1.00E+03	4.54E-05	0.00E+00	1.00E+02	5.07E-06	0.00E+00	1.00E+01

Table 3.4- Deposited mass on the heat structures after one week

### 3.4 Conclusions

Some preliminary conclusions can be derived from this first part of the proposed study on the processes driving the evolution of the simulated aerosol system:

- the agglomeration process plays a major role in the dynamic behaviour of the aerosol population. This results in the independence of the suspended aerosol mass from the initial particle size when the instantaneous release of a monodisperse aerosol source with diameters in the range 0.001-1.0  $\mu\text{m}$  is considered.
- The dominance of aerosol deposition due to gravitational settling with respect to deposition due to Brownian diffusion for all considered size ranges (remind which ones).
- One week into the transient there is almost no difference in suspended aerosol mass of initial releases in the range 10-1000 kg.

The study of the influence of different initial quantities of mass points at the interest in considering a wide range of values for this parameter, since a higher release at transient onset does not necessarily translate into a more conservative case-study.

The obtained results indicate that the input parameters used in the simulations are interacting. It is therefore difficult to define an envelope in-containment source term for the safety analysis.

It can be concluded that an uncertainty analysis approach is better suited for the task.

---

## Chapter 4

# Uncertainty analysis with lognormal aerosol size distribution

---

An uncertainty quantification (UQ) or nondeterministic analysis is the process of characterizing input uncertainties, forward propagating these uncertainties through a computational model, and performing statistical or interval assessments on the resulting responses. This process determines the effect of uncertainties and assumptions on the resulting responses. [19]

For UQ, some or all of the components of the input parameter vector, are considered to be uncertain as specified by particular probability distributions (e.g., normal, exponential, extreme value), or other uncertainty structures. By assigning specific distributional structure to the inputs, distributional structure for the outputs (i.e, response statistics) can be inferred.

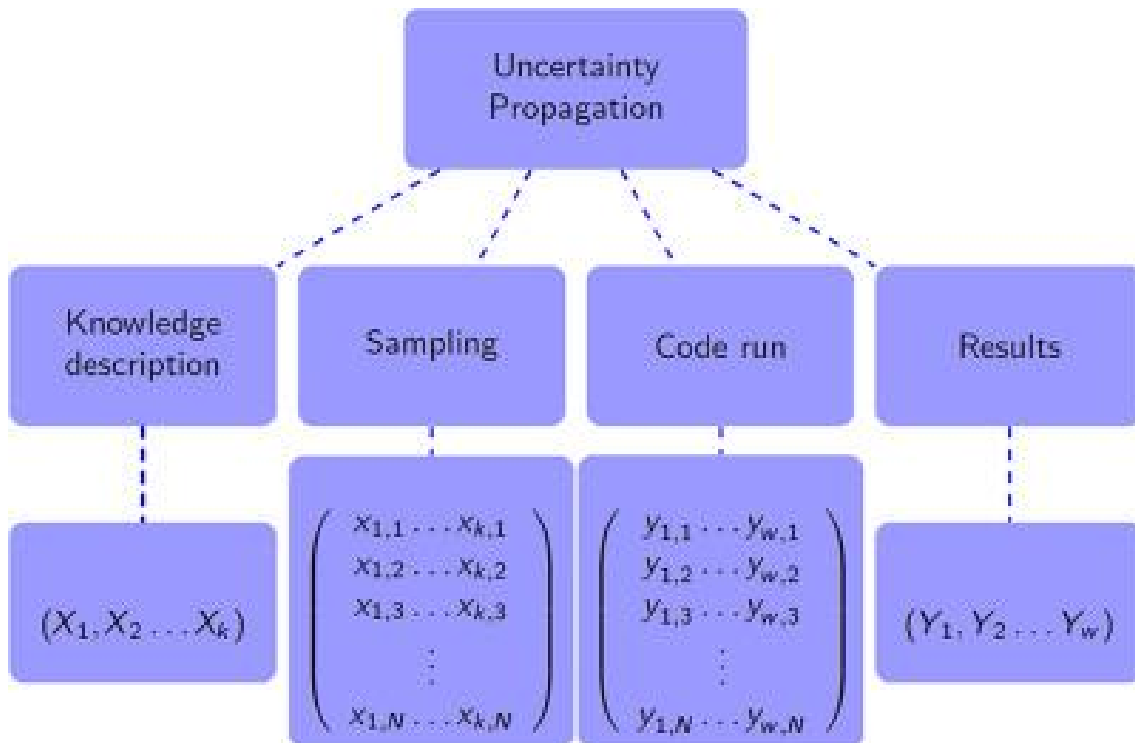


Figure 4.1- The uncertainty propagation process [20]

The necessity of an uncertainty analysis stems from the impossibility of defining with certainty the value of a parameter coupled with the ability of describing the likelihood or probability that it will fall within some specified range.

Unlike the sensitivity analysis, that attempts to describe how much model output values are affected by changes in model input values, the uncertainty analysis attempts to describe the entire set of possible outcomes, together with their associated probabilities of occurrence. [21]

This part of the study investigates, by means of an uncertainty analysis, the influence that a selected set of MELCOR input parameters has on the suspended mass of LBE aerosol in the primary containment. The suspended mass of aerosol throughout the transient is selected as the Figure of Merit (FOM) of the analysis. Its value will characterize the efficiency of aerosol removal due to natural deposition processes.

Uncertainty analyses can be performed to ensure compliance of the FOM value with the so-called 95/95 criterion, which aims at ensuring that there is a 95% probability at a 95% confidence level that some parameter does not exceed the specified acceptance limit. In the framework of nuclear safety analyses, the basis for selecting the 95% probability level is primarily for consistency with standard engineering practice in U.S. regulatory matters involving thermal hydraulics. Many parameters, most notably the departure from nucleate boiling ratio (DNBR), have been found acceptable by the NRC staff in the past at the 95% probability level. [4] Since then, the 95/95 criterion has been adopted in different international frameworks [cf. [22]].

### **4.1 Objective of the analysis**

This part of the analysis aims at experimenting methodology and tools to derive a FOM value compliant with the 95/95 criterion and to quantify the influence of selected input parameters on the FOM.

The necessity to perform an uncertainty analysis stems from the presence of uncertainties related to the modeling of the accidental scenario at study, in particular related to the aerosol source term characterization: no experimental knowledge is currently available on LBE aerosol generated by splashing upon liquid LBE impingement on structural surfaces.

### **4.2 Methodological approach**

The analysis is performed using the DAKOTA toolkit coupled with the MELCOR code in a SNAP (Symbolic Nuclear Analysis Package) environment.

The Symbolic Nuclear Analysis Package (SNAP) consists of a suite of integrated applications designed to simplify the process of performing thermal-hydraulic analysis. SNAP provides a highly flexible framework for creating and editing input for engineering

analysis codes as well as extensive functionality for submitting, monitoring and interacting with the analysis codes. [23]

DAKOTA (Design Analysis Kit for Optimization of Terascale Applications) is an open-source toolkit developed at Sandia National Laboratories, which is provided as a SNAP plug-in.

The code used for the modeling of the aerosol system is, once again, MELCOR. MELCOR code has been designed to facilitate sensitivity and uncertainty analyses through the use of sensitivity coefficients. [24]

The model implemented in MELCOR is the same used in previous simulations and described in chapter 2 and section 3.2. The number of sections is set to 20 and the size domain is expanded to 0.001-100  $\mu\text{m}$  in order to obtain more accurate results as discussed in section 3.3.3.

Figure 4.2 presents the DAKOTA workflow in SNAP coupled with the MELCOR code. Starting from a reference MELCOR input, within the SNAP environment, the uncertain parameters, their range of variation and their probability distribution are defined by the user, as well as the FOM of the analysis. DAKOTA, then, automatically generates multiple sets of input parameters. The sampling technique implemented in the UQ of this study is the Monte Carlo sampling method, where the input parameter values are selected randomly according to the user-specified probability distributions. A predefined number of MELCOR simulation runs are subsequently performed with the selected sets of input parameters. The selection of the minimum number of code runs necessary will be discussed in section 4.2.1

Finally, DAKOTA performs the statistical analysis of the sets of output obtained and characterizes the relationship between the selected uncertain parameters and the FOM. Additionally, plots of the time dependent behaviour of the variables of interest can be generated through AptPlot. [25]

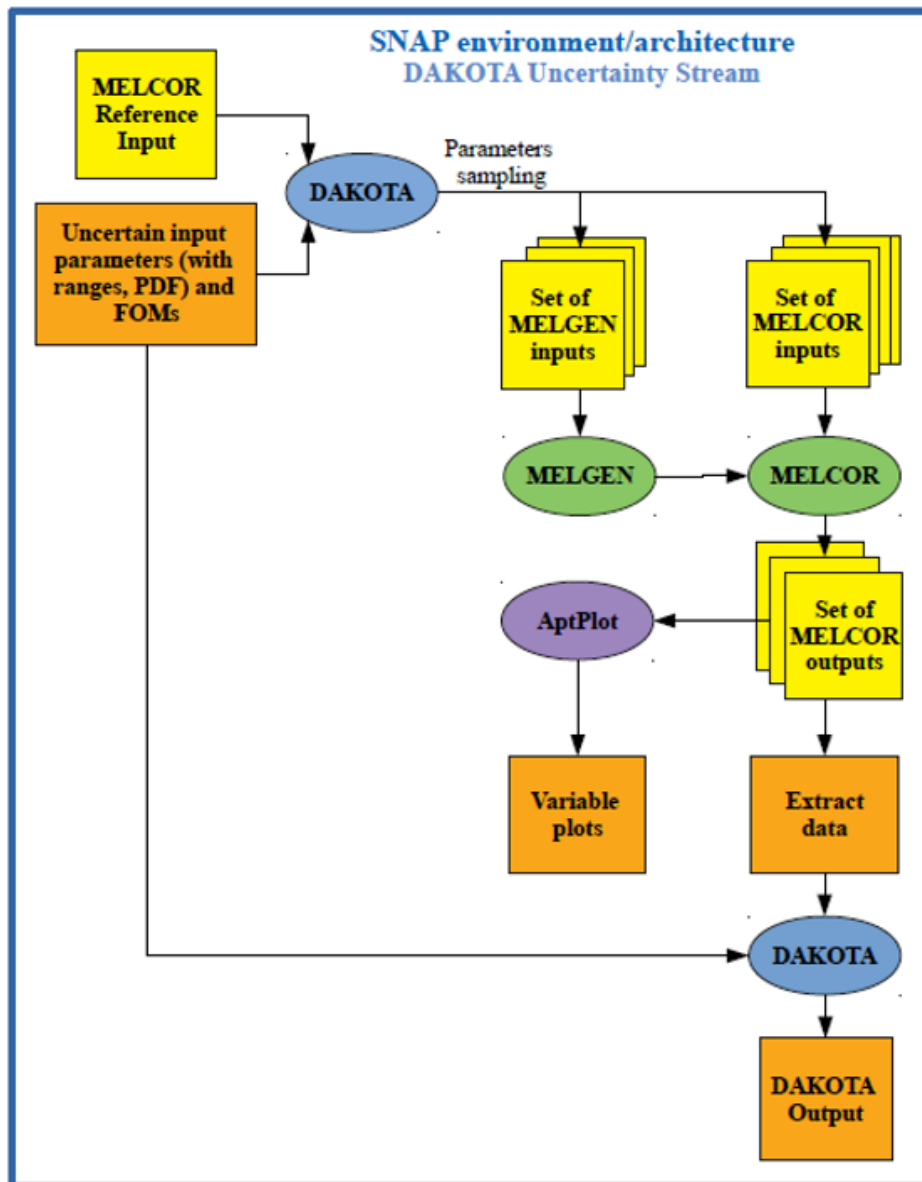


Figure 4.2- DAKOTA workflow in the SNAP environment/architecture [26]

As a result of the uncertainty analysis, DAKOTA computes correlations coefficients at multiple times during the selected one-week transient in order to describe the time dependent influence of the input uncertain parameters on the FOM of the analysis. The correlation coefficients and their interpretations will be further discussed in section 4.3.2.

As a result of the uncertainty analysis, DAKOTA computes correlations coefficients at multiple times during the selected one-week transient in order to describe the time dependent influence of the uncertain input parameters on the FOM of the analysis. The correlation coefficients and their interpretations will be further discussed in section 4.3.2.

Within the framework of this analysis the FOM is defined as a single scalar value calculated from the results of a single code run. As previously mentioned, the output value selected as FOM in this study is the suspended mass of LBE aerosol.

#### 4.2.1 Statistical considerations

In order to specify the number of code runs required to achieve the probability and confidence level required for the FOM, the approach developed by Wilks [27] is applied. Wilks' method is based on order statistics and allows to determine the minimum number of samples required to achieve a specified probability and confidence band.

The following discussion will be focused on obtaining an acceptable upper bound value, since the interest of the study is to get a conservative estimate of the quantity of suspended mass in the primary containment, which represents the source term of the accidental scenario at study.

Given a statistical sample, the probability that its  $i^{\text{th}}$  order statistics ( $Y_i$ ) is greater than the  $p^{\text{th}}$  percentile value of the distribution ( $\pi_p$ ) can be stated as:

$$P(Y_i > \pi_p) = 1 - \sum_{k=i}^n \binom{n}{k} p^k (1-p)^{n-k} = 1 - \alpha \quad (4.1)$$

The confidence level is then  $(1 - \alpha)$ , where  $\alpha$  is the level of significance.

Starting from this formulation Wilks back-calculated the number of sample size required ( $n$ ) to make the statistical statement true.

The probability that the maximum value in a sample of size  $n$  is greater than a particular the  $p^{\text{th}}$  percentile value of the distribution is simply:

$$P(Y_i > \pi_p) = 1 - p^n = 1 - \alpha \quad (4.2)$$

The sample size can then be derived as

$$n = \frac{\ln(\alpha)}{\ln(p)} \quad (4.3)$$

In the proposed study the compliance to the 95/95 criterion is required for the upper bound value of the FOM. Therefore, the percentile value  $p$  is equal to 0.95 and the level of significance  $\alpha$  is 0.05. When 1<sup>st</sup> order statistic is applied for a single FOM, a minimum sample size of 59 simulation runs is required. The sample size does not carry any dependence on the number of uncertain input parameters.

With 59 runs, the upper bound value of the resulting distribution of results will have a 95% probability of being higher than the actual 95<sup>th</sup> percentile value.

#### 4.2.2 Selection of uncertain parameters

In order to determine the final selection of the most significant uncertain input parameters for the uncertainty analysis, a literature review was performed. No information specific to the aerosol material and aerosol generation mechanism at study could be found, but some general indications could be derived to support the selection. It is reminded that this part of the study aims at experimenting methodology and tools to derive a FOM value compliant with the 95/95 criterion and to quantify the influence of selected input parameters on the FOM, rather than at performing a complete and fully representative uncertainty analysis for the accident scenario at study. For such purpose, it is deemed acceptable to use range of variations and statistical distributions of input parameters not specifically derived for LBE aerosols.

The uncertain parameters investigated are the ones defining the particle size distribution of the aerosol source, namely the mass average of the size distribution and the geometric standard deviation.

Additionally, other parameters considered are the ones related to agglomeration, since, as previously observed in the sensitivity analysis, it is a process that highly characterizes the dynamic behaviour of the aerosol. These parameters are the dynamic shape factor, the agglomeration shape factor and the quantity of LBE mass released.

Finally, some brief considerations are dedicated to a parameter characterizing the diffusive deposition process, that is the diffusion layer boundary thickness.

##### 4.2.2.1 Particle size distribution

Since the number density of aerosol particles can be huge, it is quite impossible to predict aerosol behaviour by calculating the dynamics of individual particles. Therefore, aerosol must be considered in a collective sense, and the aerosol is taken to have some continuous distribution of particles. Such distribution is conventionally described as lognormal distribution. The lognormal distribution has no theoretical basis for its application to aerosols, but it has been empirically observed to represent a good fit for most single-source aerosols. [28]

All related information that will be presented in the following literature review assumes such distribution.

In order to better comprehend the data presented in the following discussion, a brief explanation of the different types of equivalent diameters and weighted averages, as well as a small introduction to the lognormal distribution, is given.

Values of interest in the current analysis are the count median diameter (CMD), that in a lognormal distribution corresponds to the geometric mean diameter, and the mass median

diameter (MMD). The CMD is defined as the diameter for which one-half of the total number of particles are smaller and half-one are larger and the MMD, as previously defined in section 3.3.1, is the diameter for which half of the mass is contributed by particles larger than MMD and half by particles smaller than the MMD.

Additionally, the definition of the aerodynamic mass mean diameter (AMMD) is given, since experimental results are often reported in literature in these terms.

In the distribution of an aerosol population that has been sorted into a series of successive size intervals (sections), the geometric mean diameter ( $d_g$ ) can be defined as

$$d_g = \exp \left[ \frac{\sum n_i \ln d_i}{N} \right] \quad (4.4)$$

where  $n_i$  is the number of particles in section  $i$  having midpoint diameter  $d_i$  and  $N$  is the total number of particles in the sample.

The value for the AMMD can be defined starting from the formulation of the geometric mass mean diameter (GMMD):

$$GMMD = \frac{\sum m_i d_i}{M} \quad (4.5)$$

where  $m_i$  is the mass of all the particles in section  $i$  having midpoint diameter  $d_i$  and  $M$  is the total mass for all sections.

The aerodynamic diameter ( $d_a$ ) is the diameter of the unit density ( $\rho_0$ ) sphere that has the same settling velocity as the irregular particle.

Therefore, the mass mean diameter can be converted into AMMD by multiplying for the root of the ratio between the particle density ( $\rho_p$ ) and unit density ( $\rho_0$ ):

$$AMMD = GMMD \sqrt{\frac{\rho_p}{\rho_0}} \quad (4.6)$$

As previously anticipated, the lognormal distribution is used extensively for aerosol size distributions because it fits the observed size distributions reasonably well.

A lognormal distribution is completely defined by a CMD and a geometric standard deviation (GSD) (the standard deviation of the logarithm) defined as:

$$GSD = \exp\left(\sqrt{\frac{\sum n_i (\ln d_i - \ln d_g)^2}{N - 1}}\right) \quad (4.7)$$

where  $n_i$  is the number of particles in group  $i$  having midpoint diameter  $d_i$ , geometric mean diameter  $d_g$  and  $N$  is the total number of particles in the sample.

It must be reminded that for a lognormal distribution the geometric mean diameter  $d_g$  coincides with the count mean diameter, CMD. Therefore, the frequency function can be expressed as:

$$df = \frac{1}{\sqrt{2\pi} d_p \ln GSD} \exp\left[-\frac{(\ln d_p - \ln CMD)^2}{2(\ln GSD)^2}\right] dd_p \quad (4.8)$$

where  $d_p$  is the particle diameter.

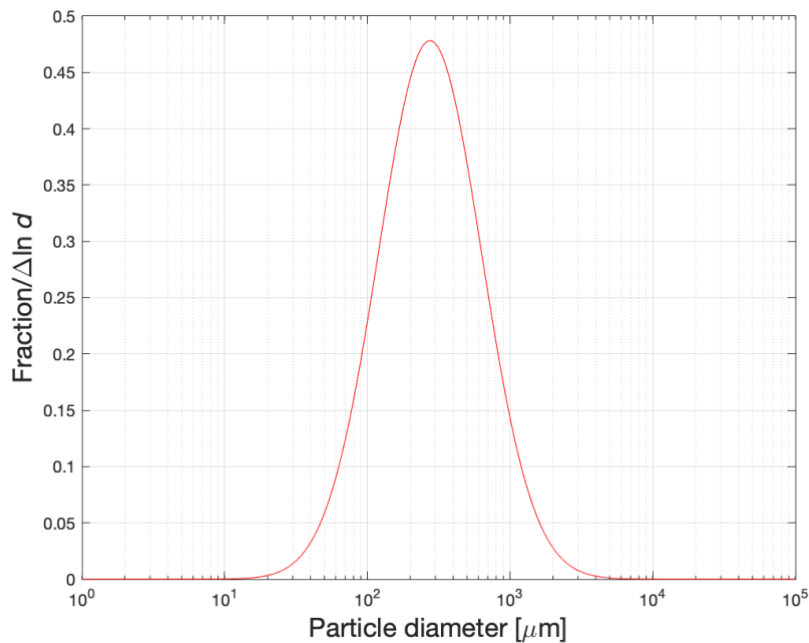


Figure 4.3- Frequency distribution curve

For a lognormal distribution, the distribution is normal with respect to the natural logarithm of the particle diameter so that 95% of the particles fall within a size range defined by

$$\exp[\ln CMD \pm 2 \ln GSD] \quad (4.9)$$

This range is asymmetrical and goes from  $CMD/GSD^2$  to  $CMD \cdot GSD^2$ .

All weighted distributions of any lognormal distribution will be lognormal and have the same geometric standard deviation. Therefore, the distribution of count and mass will have the same shape when plotted on a logarithmic scale, but the mass distribution will be displaced along the size axis by a constant amount equal to the ratio  $MMD/CMD$ . [28]

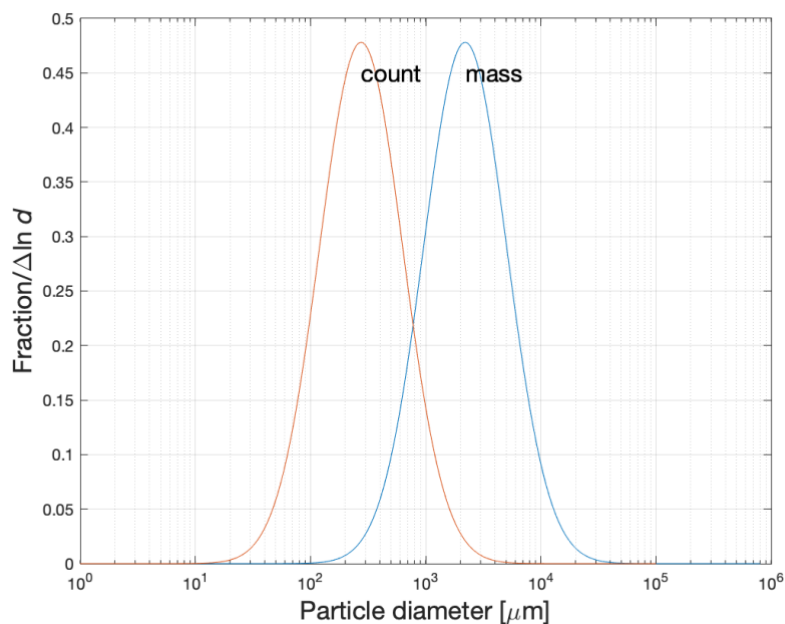


Figure 4.4- Example of a count and mass lognormal distribution

As previously mentioned, experimental results related to LBE aerosol generation due to mechanical process are not currently available in literature. For the purpose of the present study, values describing the particle distribution of aerosol particles generated in sodium fires (derived from literature relative to Sodium Fast Reactor accident analysis) are taken as reference values. The underlying assumption is that the aerosol generated by the combustion processes that characterize sodium fires would be either equal or smaller in size compared to LBE aerosol generated by mechanical impact. This assumption requires further substantiation; a dedicated experimental campaign is currently on-going at SCK CEN to characterize the LBE aerosol source.

In literature, values for the AMMD generated by sodium fire can be found ranging from 0.5  $\mu\text{m}$  to 4.0  $\mu\text{m}$  with GSD assuming values from 2 up to 3 [29]. In some cases, the values for AMMD are reported to reach maximum values of 6  $\mu\text{m}$  [30].

Measurements of sodium combusted aerosol at different relative humidity resulted into values of MMD ranging from 1.3  $\mu\text{m}$  up to about 1.8  $\mu\text{m}$  right after generation [31]. Studies aimed at modeling the behaviour of sodium aerosol propose MMD values to vary in the range 0.5-4  $\mu\text{m}$  and GSD values in the range 1.5-3 [32].

Both the mass averages of the particle size distribution and the GSD are chosen as uncertain input variables for the uncertainty analysis due to the impossibility of selecting set values that are deemed to reliably describe the size distribution of the LBE aerosol under investigation.

##### 4.2.2.2 Dynamic shape factor

The dynamic shape factor is used to correct the equations describing Stoke's law to take into consideration the departure from idealized conditions in which the particles are considered spherical as discussed in section 2.2.2. Larger values of the dynamic shape factor reduce the two agglomeration kernels contributors (equations 2.17 and 2.18), therefore they give a negative contribution to the agglomeration rate.

Once again, in absence of experimental data relevant to the specific conditions at study, literature sources relative to SFR and LWR reactor accident analyses were consulted to derive indications over possible ranges of variation for this parameter. Measurements of sodium aerosol resulted in dynamic shape factors between 2 and 4 [33] and in values very close to the unity [31] [34]. Additionally, range of values of 1-5 can be found in LWR studies proposing uncertainty analyses [35] and mean values of 1.85 and 2.25 are reported for measurements of fission aerosols in LWR technology [36]. In particular reference [35] identifies this parameter as relevant for the study of in-containment aerosol deposition behaviour. The dynamic shape factor is therefore retained as uncertain parameter for our uncertainty analysis.

##### 4.2.2.3 Agglomeration shape factor

The agglomeration shape factor ( $\gamma$ ) accounts for the greater spatial extent of nonspherical particle during coagulation processes. A unit value of the agglomeration shape factor expresses the uniformity of the density of the aerosol particles with the bulk density of the material. All agglomeration processes are enhanced by large values of the agglomeration shape factor, as it can be observed in the equations 2.17 and 2.18 that show the proportionalities of the agglomeration kernels.

Since a value equal to unity minimizes the aerosol agglomeration rate, which is conservative for the safety analysis of the event (leading to slower deposition), this parameter will be attributed a value of one and will not be further considered as an uncertain parameter in the uncertainty analysis.

### 4.2.2.4 LBE aerosol mass released

The LBE aerosol mass released, in the model applied in this analysis, is directly correlated to the initial concentration of aerosol in the containment atmosphere since the aerosol mass inventory is homogeneously (and instantaneously) released into the control volume. The quantity of aerosol generated by the impingement on solid surfaces of liquid LBE will be dependent upon accident conditions (such as, for instance, size of the LBECS break from which the LBE spill originates and drop height) over which currently not enough information is available.

the variation of quantity of aerosol mass released has already shown, in the previous chapter, its influence on the suspended aerosol in the first phases after accident onset, we therefore retain this parameter as an input variable of the uncertainty analysis.

### 4.2.2.5 Diffusive layer boundary thickness

The diffusive boundary layer ( $\delta_D$ ) is the effective thickness across which aerosol particles are deposited by Brownian concentration diffusion onto walls.

Even though the diffusive boundary layer thickness presents a possible range of variation reported in literature [32], the small influence of the deposition process due to Brownian motion with respect to deposition by gravitational settling for our specific case study (as highlighted in section 3.3.3) reduces the interest in observing the influence of this parameter on the value of suspended mass, since it is expected to be minimal. Therefore, it is not retained as an uncertain parameter for the following uncertainty analysis.

## 4.2.3 Range of variation and statistical distribution of uncertain parameters

Out of the parameters investigated in the previous section, the values for the mass weighted diameters, the geometric standard deviation, the dynamic shape factor and the LBE mass released are selected as uncertain parameters for the uncertainty analysis.

From the findings of the literary review presented in the previous section, a reasonable range of variation for the AMMD for sodium-based aerosol is established to be 1-4  $\mu\text{m}$ . If we want to apply this range of values to LBE aerosols, the AMMD has to be corrected for the different density of LBE compared to sodium and sodium oxides, as shown in equation 4.6. The resulting range obtained for the AMMD of LBE aerosol is 2-9  $\mu\text{m}$ . According to MELCOR User's Guide [14], the input regarding the mass weighted diameter of the aerosol distribution must be provided in terms of AMMD. There is reason to believe that the code rather interprets the provided AMMD values as MMD. This aspect will be discussed in Appendix A. For the following discussion, we will consider that the uncertain parameter whose variation is considered is the MMD. This issue is not expected to alter the conclusions of the present study.

As for the values of the geometric standard deviation of the lognormal distribution of aerosol particles, the range has been chosen to cover the data found in literature on LWR and SFR accident analysis. The GSD is, thus, set to vary from 1.2 to 3.

The review of the dynamic shape factor resulted in the definition of a range going from the unit value up to 5, which represent a relatively high value when different literature sources are considered (it is reminded that a high dynamic shape factor is conservative with regard to the considered FOM).

It is hard to define the aerosolized fraction of the LBE inventory spilling into the Primary Containment in case of leakage or breakage of the LBECS. A range of 1-250 kg has been chosen by engineering judgment.

The following table summarizes the ranges selected for the set of uncertain parameters.

<b>Parameters</b>	<b>Range</b>
Mass median diameter (MMD)	2-9 $\mu\text{m}$
Geometric standard deviation (GSD)	1.2-3
Dynamic shape factor	1-5
LBE aerosol mass released	1-250 kg

*Table 4.1- Ranges of variation of uncertain parameters*

In absence of more detailed information, the probability distribution of each of the input parameters within the considered range of variation is chosen to be uniform. Additionally, no correlations among the input variables are provided and all parameter values are assumed to be independent.

### **4.3 Results**

The modeled aerosol source releases the entirety of the aerosol mass inventory into the control volume during the first second of the transient; the transient duration is set to a week.

The uncertainty analysis performed with DAKOTA in the SNAP environment produces a report that includes the sampled input values of the uncertain parameters for all the simulation runs and the resulting values for the evolution of the suspended mass.

#### **4.3.1 Values of FOM**

The following graphs (Figure 4.5) shows the evolution during the one-week transient of the minimum, maximum, mean and median values of the FOM (i.e. the suspended mass of LBE aerosol) among the results of the 59 simulation runs.

As discussed in section 4.4.1, the maximum values of the FOM are the ones of main interest in this study since they allow compliance with the 95/95 criterion required.

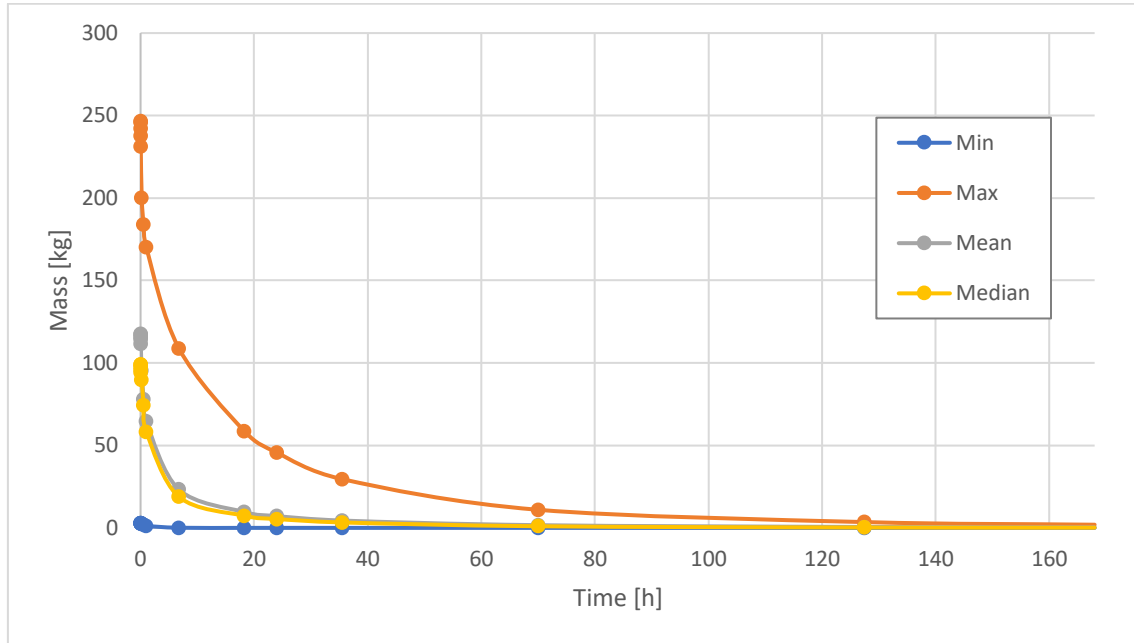


Figure 4.5- Results for the suspended mass in the uncertainty analysis

If the interest is placed on the ability of the natural deposition processes to remove the initially suspended particles, the decontamination factor is a parameter of interest.

The decontamination factor (DF) is defined as the ratio between the initial mass released and the suspended mass at a given moment in time. It is a good indicator of the removal efficiency of aerosol from the containment atmosphere.

In the Table 4.2 the most conservative values, corresponding to the upper bound values of the FOM, are recorded. They highlight the exponential increase in the aerosol depletion capabilities of the system.

Time	1st order
	DF
1 day	4.43
1 week	101.32

Table 4.2- Values of the decontamination factor

Figure 4.6 shows the time dependent values of the FOM for each of the 59 simulation runs performed.

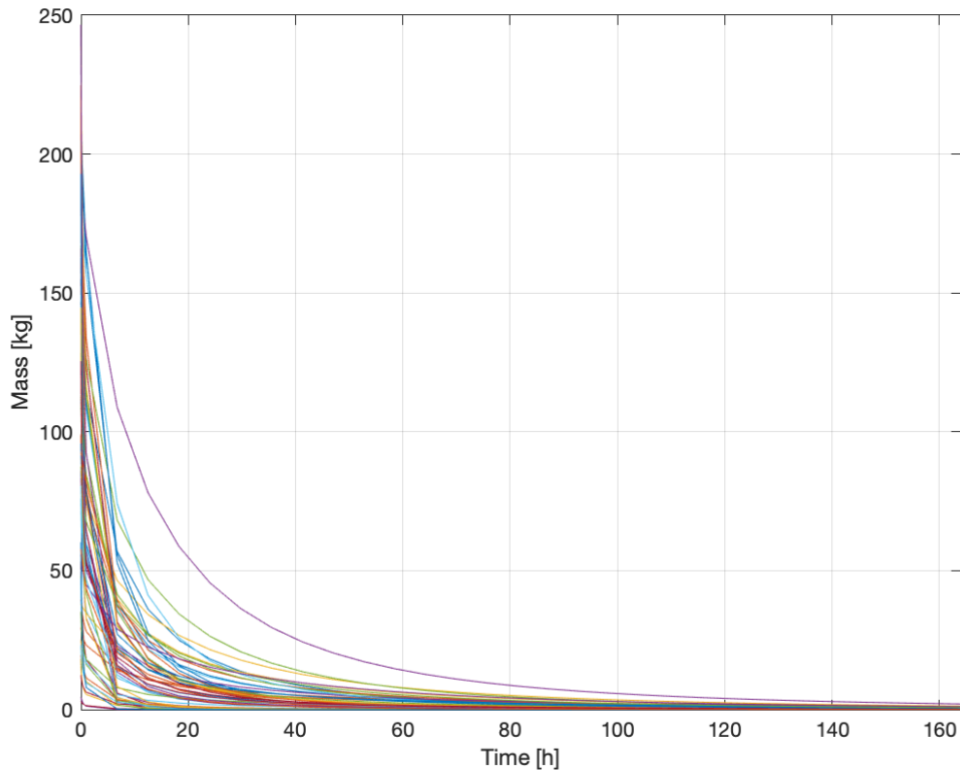


Figure 4.6- Suspended mass for the 59 simulation runs

### 4.3.2 Correlation coefficients- Explanation and values

In order to assess the influence of the single input parameter variation on the FOM, the values of two specific correlation coefficients are recorded throughout the transient duration:

- Pearson's correlation coefficient- Measures the strength and direction of linear correlation between two variables. The correlation is performed on actual input and output data. Its value can vary between +1, for a perfect increasing linear relationship, and -1, for a perfect decreasing linear relationship.
- Spearman's correlation coefficient- Measures the strength and direction of monotonic relationship between two variables. Once the input and output data are sorted in ascending order (ranked), it calculates the correlation between the same rank of input and output data. Its value, ranging from +1 to -1, indicates the association of ranks.

Formulation of the correction coefficient ( $\rho$ ) defined for two variables  $x$  and  $y$ , in this analysis, respectively, the value of a single input parameter and the FOM:

$$\rho = \frac{\sum_i (x_i - \bar{x})(y_i - \bar{y})}{\sqrt{\sum_i (x_i - \bar{x})^2 \sum_i (y_i - \bar{y})^2}} \quad (4.10)$$

For values of the correlation coefficients greater than 0.5 the correlation is considered significant, if they are between 0.2 and 0.5 the correlation is moderate, otherwise it is low. [37]

Figures 4.7 and 4.8 show, respectively, the values of the Pearson's coefficient and the Spearman's coefficient in a logarithmic time scale.

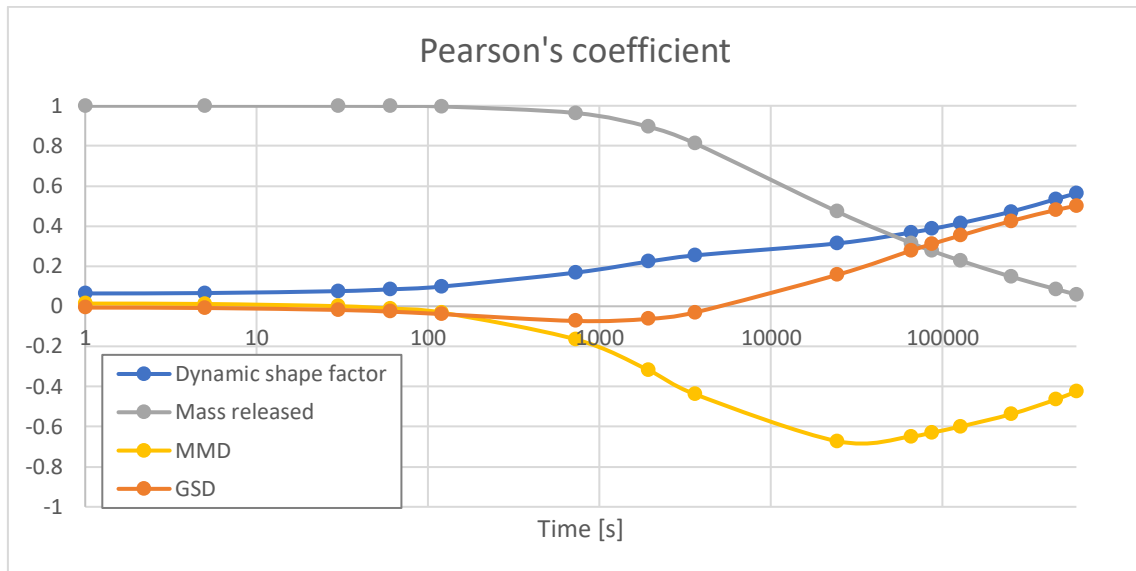


Figure 4.7- Values of Pearson's correlation coefficient throughout the transient

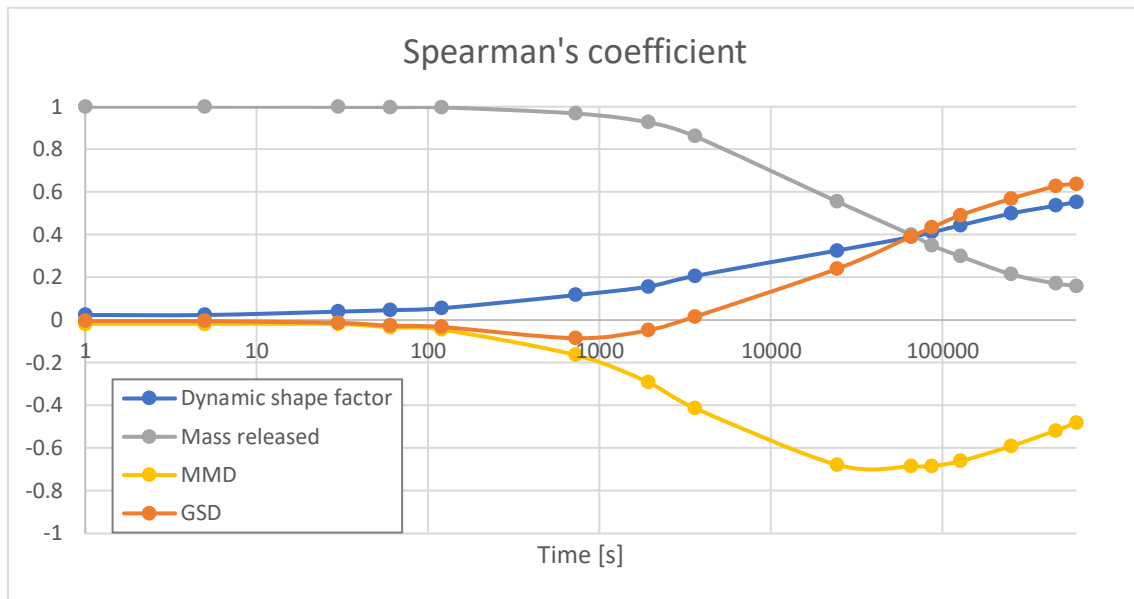


Figure 4.8- Values of Spearman's correlation coefficient throughout the transient

We can draw the following conclusions:

- The influence of the quantity of mass released dominates the first phase of the transient, where higher mass released directly translates to higher quantity of suspended mass. With the evolution of the transient, it increasingly loses its influence on the FOM, until reaching the point of having little to no correlation with the suspended mass at the end of the weeklong transient.
- The dynamic shape factor shows a higher influence on the suspended mass at a later phase of the transient, once the average particle size is reduced due to the deposition of bigger sized particles.
- The values for the correlation coefficients for the MMD and GSD indicate the high influence of smaller particles on the FOM towards the end of the transient. For the same aerosol mass, a high GSD value translates into a larger quantity of small particles released at transient onset; these small particles are the ones that remain airborne at the end of the transient (as their gravitational deposition is slow), resulting in a gradually increasing value of the correlation coefficients for the GSD parameter. A similar observation can be made for the MMD, where lower values directly correlate to particles released in a lower size range which, as it was observed for the GSD, remain airborne longer due to their slow gravitational deposition. This correlation is observed in the negative values of the correlation coefficients which indicate a decreasing relationship, when a higher MMD input value results in a lower FOM.

The following table shows the numerical values for both correlation coefficients after one hour, one day and one week from the accident onset. The correlations between input and

output values at the time during the transient when are shown to be most relevant by the correlation coefficients are reported in Figure 4.9 and 4.10.

Time	Dynamic shape factor		Mass released		MMD		GSD	
	PC	SC	PC	SC	PC	SC	PC	SC
1 h	0.25	0.21	0.81	0.86	-0.44	-0.41	-0.03	0.02
24 h	0.39	0.41	0.28	0.35	-0.63	-0.68	0.31	0.43
1 week	0.56	0.55	0.06	0.16	-0.42	-0.48	0.50	0.64

Table 4.3- Values for Pearson's correlation coefficient (PC) and Spearman's correlation coefficient (SC)

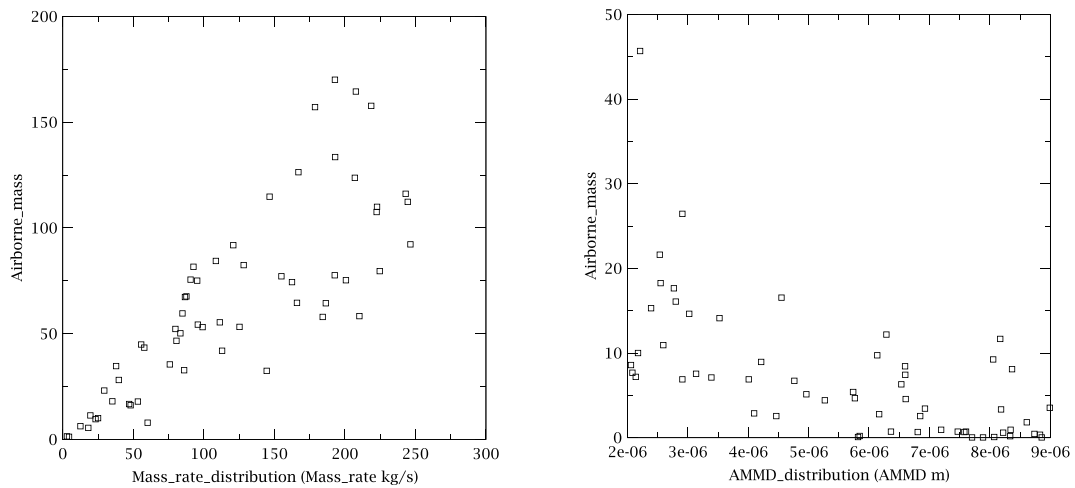


Figure 4.9- Correlation between the mass released and the suspended mass after 1 hour from the start of the transient (on the left). Correlation between the MMD and the suspended mass after 1 day from the start of the transient (on the right).

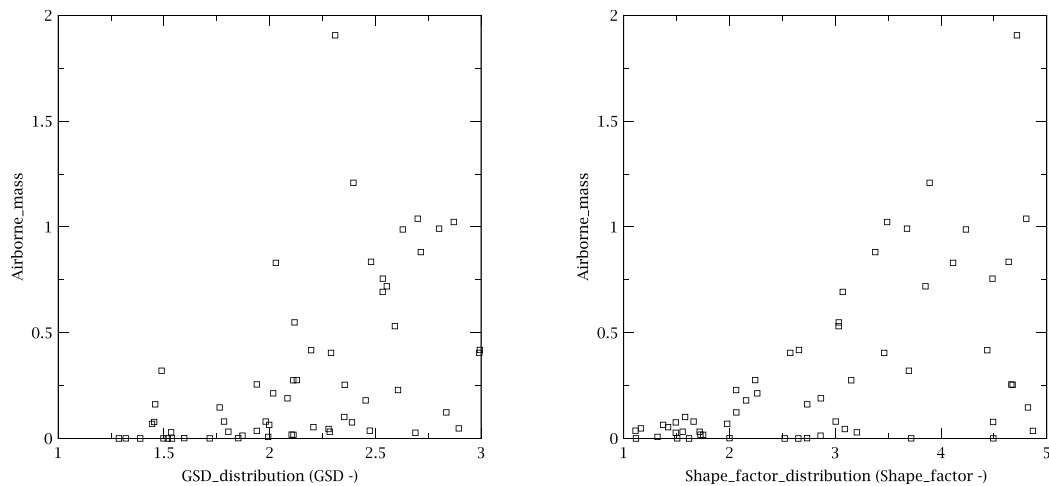


Figure 4.10- Correlation between the GSD and the suspended mass after 1 week from the start of the transient (on the left). Correlation between the dynamic shape factor and the suspended mass after 1 week from the start of the transient (on the right).

### 4.3.3 Higher order statistics

The maximum FOM value of the sampling distribution of the maximum value in a sample of 59 code runs (Figure 4.11) will be greater than the 95<sup>th</sup> percentile value of the distribution 95% of the time.

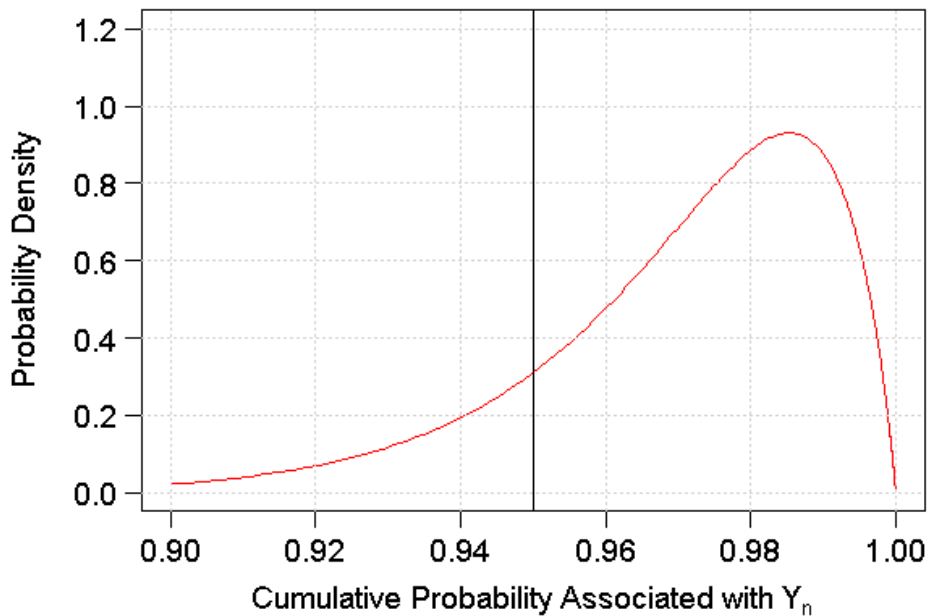


Figure 4.11- Sampling distribution of the maximum value in a sample of 59 used for estimating the 95th percentile value with 95% confidence [23]

To improve the estimation of the upper bound value, it is possible to perform a higher number of simulations and then choosing a different order statistic as the estimate.

Starting from the same equation for the upper bound confidence limit (equation 4.1), one can back-calculate the required sample size for different order statistics ( $m^{\text{th}}$  highest) at a given confidence level. [38]

The interest in investigating higher order statistics arises from the knowledge that using the minimum number of simulations required by Wilks (59), there is a high likelihood that the estimated FOM is much higher than the true 95th percentile value. Therefore, the upper bound estimate may be too conservative. To improve this estimation, a higher order statistic can be implemented in the uncertainty quantification.

The graph and table reported below show the distribution of the  $m^{\text{th}}$  highest value and the associated sample size required. Therefore, by setting a higher order statistics, a higher number of simulations is required and a better estimate of the 95th percentile of the FOM can be obtained.

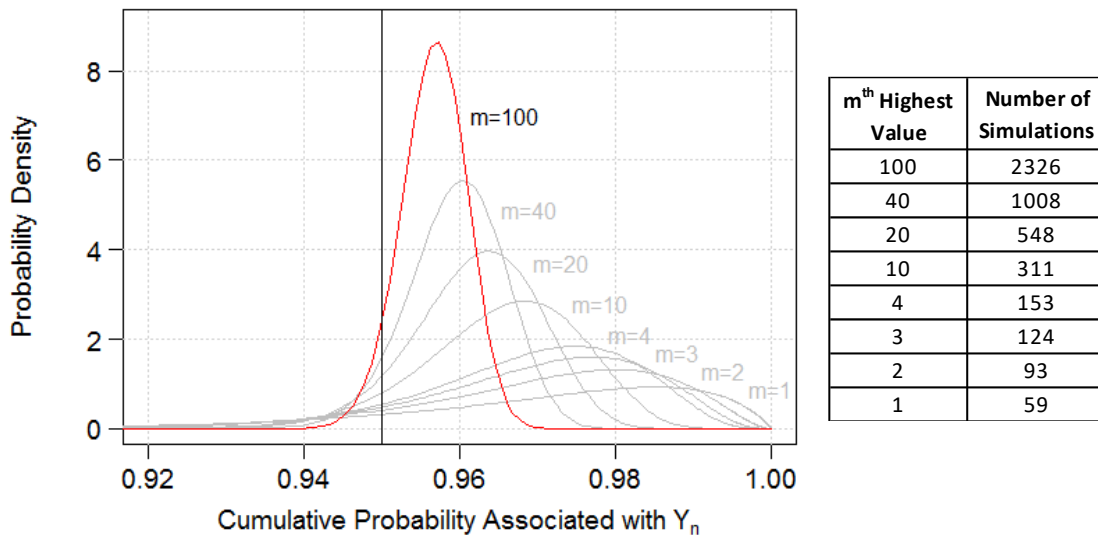


Figure 4.12- Sampling distribution and sample size of the  $m^{\text{th}}$  highest values required for estimating the 95th percentile value with 95% confidence [23]

The quantification of values of FOM is performed once again, but using 3<sup>rd</sup> order statistic and calculating the new sample size to ensure compliance with the 95/95 criterion for the upper limit. The updated sample size is 124 simulation runs.

Results shown in Figure 4.13 are the maximum values of the FOM in two different UQ, one performed with 1<sup>st</sup> order statistics (highest FOM value out of 59 code runs) and the other with 3<sup>rd</sup> order statistics (third-highest FOM value out of 124 code runs).

The values for the higher order statistic, as expected, are shown to be lower throughout almost the whole transient.

The results obtained with third order statistics give a slightly less conservative estimate of the upper bound value of the FOM, but no major impact is observed. The analysis based on 1<sup>st</sup> order statistic is therefore deemed appropriate.

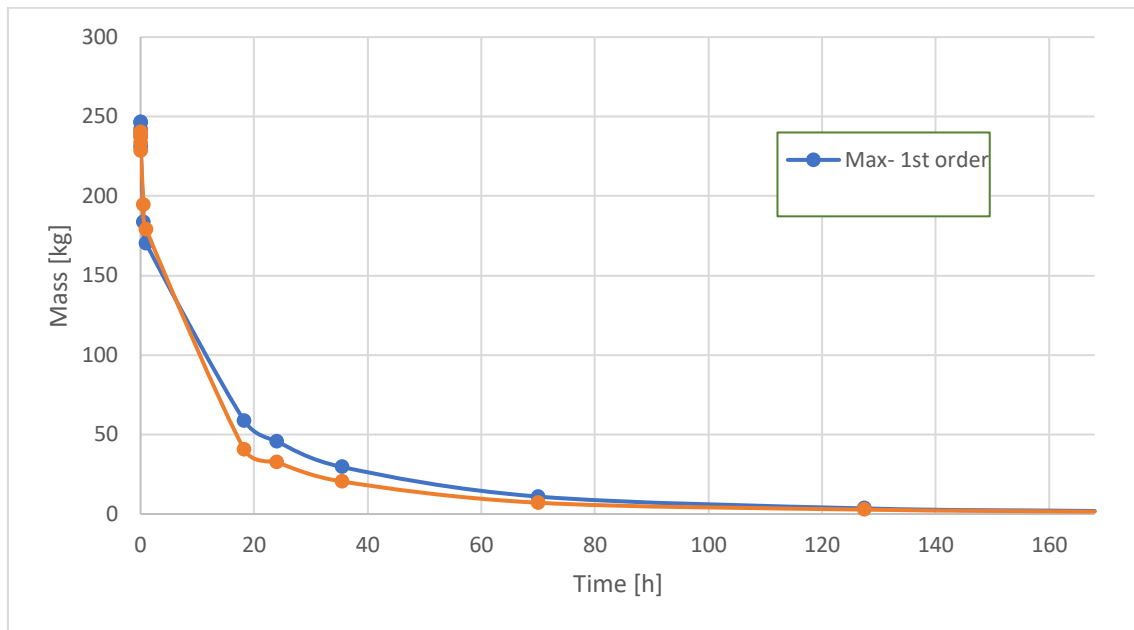


Figure 4.13- Maximum values of suspended mass obtained with 1<sup>st</sup> and 3<sup>rd</sup> order statistic

	Suspended mass after a week (kg)
<b>1st order</b>	1.905
<b>3rd order</b>	1.485

Table 4.4- Values for the suspended mass with 1<sup>st</sup> and 3<sup>rd</sup> order statistic

#### 4.4 Conclusions

- Input parameter with the highest influence on the FOM during the transient:
  - 0-1h after accident onset: LBE mass released;
  - 1-24h after accident onset: Mass Median Diameter of generated aerosol;
  - 24h-168h after accident onset: Dynamic shape factor and Geometric Standard Deviation gradually become dominant.
- The implementation of higher order statistic in the UQ effectively produces better estimate of the upper bound values of the FOM in compliance with the 95/95 criterion. For a 3<sup>rd</sup> order statistics, the impact on the FOM with respect to a first order statistics remains limited.

---

# Chapter 5

## Mitigation strategy

---

In the previous chapters, the dynamic behaviour of an in-containment radioactive heavy liquid metal aerosol source has been the focus of the analyses. Starting from the results obtained, a possible mitigation strategy is developed in order to reduce the mass of radioactive aerosol suspended in the containment atmosphere.

### 5.1 Hypothesis to investigate

In the previous parts of the study, it was observed that the agglomeration process highly characterizes the dynamic behaviour of the system. Furthermore, bigger sized particles, in part generated through the agglomeration process, are more efficiently removed from the atmosphere due to the gravitational deposition, which was observed to be the main deposition process in the modeled system.

Starting from these conclusions, a proposal for a possible mitigation strategy is developed. The mitigation strategy would consist in the injection of non-radioactive aerosol particles at a certain moment during the transient, in order to enhance the deposition rate of radioactive aerosol by exploiting the agglomeration of the newly introduced particles with the ones already suspended in the containment atmosphere. The hypothesis made is that bigger particles would be generated through agglomeration and facilitate the removal of airborne radioactive aerosol through gravitational deposition. The additional injection of aerosol material is expected to result in the reduction of suspended radioactive aerosol in the containment atmosphere.

This analysis aims both at confirming and quantifying the efficacy of the proposed mitigation strategy and at finding the optimum characteristics of the injection.

### 5.2 Reference case

In order to test the efficacy of the proposed mitigation strategy, a reference case (in terms of characteristics of the aerosol source) is chosen.

The selected reference case is the one that generates the most conservative results in the uncertainty analysis performed in the previous chapter.

The specific parameters that characterize the selected aerosol source are reported in the Table 5.1.

<b>Dynamic shape factor</b>	4.7
<b>Mass released</b>	193.0 kg
<b>MMD</b>	2.2 $\mu\text{m}$
<b>GSD</b>	2.3

Table 5.1- Reference case

Figure 5.1 shows the mass distribution of the aerosol source of the reference case. The mass distribution is displayed as the quantity of mass released into each of the size bins that discretize the size domain.

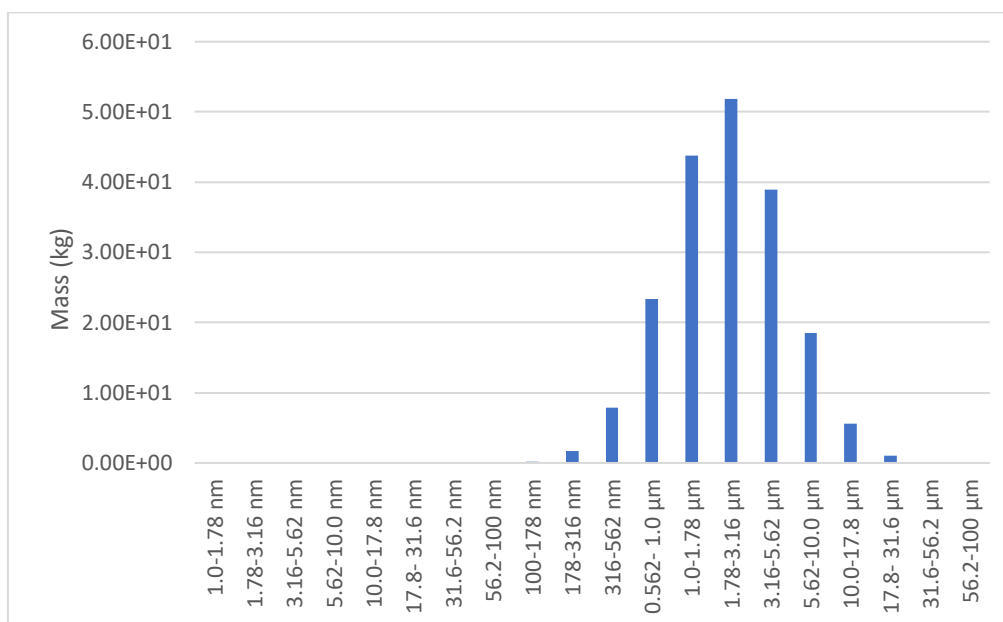


Figure 5.1- Mass distribution of radioactive source of reference case

For the reference case, when no mitigative action is considered, the suspended mass of radioactive aerosol after a week is **1.885 kg**. The influence of the non-radioactive LBE aerosol injection on this FOM is the focus of this part of the analysis.

### 5.3 Characteristics of the injection

The injection of LBE particles with identical characteristics (namely density) to the particles that constitute the in-containment aerosol source, except for the lack of radioactivity, is considered as mitigating action. The choice of LBE as the injected material is imposed by code limitations restricting the user to consider a single value for the density of all components of the system (as mentioned in section 2.2.3).

In MELCOR, a new component is introduced to model non-radioactive LBE aerosol.

The non-radioactive mass is set to be injected in a single, pre-selected size bin as monodisperse source. The non-radioactive injected aerosol is instantaneously and homogeneously distributed in the control volume atmosphere. The total mass of the mitigating aerosol source is injected over 10 seconds at a constant rate.

The timing of injection and the injected particle size, as well as the quantity of injected mass necessary to have a consistent impact on the suspended radioactive mass, are the parameters investigated in the following analysis. Their influence on the depletion of radioactive aerosol is observed on the quantity of suspended radioactive mass a week after the accident onset.

### 5.4 Results

Starting from the reference case, several simulation runs are performed where non-radioactive LBE aerosol mass is injected with different particle sizes and at different time throughout the transient. The results are presented and analyzed in the following sections.

#### 5.4.1 Injection 72h after the accident onset, in a wide range of size values

The first results obtained cover a wide range of injected particle sizes, for two different values of non-radioactive LBE mass introduced (10 kg and 100 kg). All injections are introduced 72 hours after the initial release of the radioactive LBE source. Results are summarized in Table 5.2.

The injection of non-radioactive LBE aerosol shows to be more effective in reducing the suspended radioactive aerosol mass when smaller sized particles are injected. This is due to the following reasons:

- Smaller particles remain airborne for longer, due to slower gravitational settling, therefore their impact on the overall agglomeration process is greater.
- For a given injected aerosol mass, reducing the size of the injected particles translates into higher particle number density, thus increasing the rate of agglomeration (as described by equation 2.3).

It should be stressed that the objective of the proposed mitigation strategy is solely to reduce the radioactive mass in suspension and not the overall quantity of suspended aerosol mass.

From the presented results it can be concluded that, to produce a relevant effect, the injected mass should at least be in the order of 100 kg.

Furthermore, it can be observed that particles larger than a few  $\mu\text{m}$  are ineffective for mitigation and their introduction has a negligible impact on the suspended quantity of radioactive LBE aerosol.

Size bin in which the non-radioactive aerosol is released	Ratio MMD introduced/ MMD already present	Suspended mass after 1 week (kg)			
		Release of 100 kg of non-radioactive LBE		Release of 10 kg of non-radioactive LBE	
		Radioactive aerosol	Total aerosol	Radioactive aerosol	Total aerosol
178-316 nm	0.17	0.367	8.080	1.437	5.316
316-562 nm	0.30	0.371	8.050	1.448	5.280
0.562- 1.0 $\mu\text{m}$	0.53	0.386	7.783	1.468	4.825
1.0-1.78 $\mu\text{m}$	0.95	0.489	5.565	1.561	3.112
1.78-3.16 $\mu\text{m}$	1.69	0.963	1.370	1.726	1.802
3.16-5.62 $\mu\text{m}$	3.00	1.624	1.624	1.852	1.852
5.62-10.0 $\mu\text{m}$	5.33	1.835	1.835	1.880	1.880
10.0-17.8 $\mu\text{m}$	9.48	1.876	1.876	1.884	1.884
17.8- 31.6 $\mu\text{m}$	16.86	1.884	1.884	1.885	1.885
31.6-56.2 $\mu\text{m}$	29.97	1.885	1.885	1.885	1.885
56.2-100 $\mu\text{m}$	53.30	1.885	1.885	1.885	1.885

Table 5.2- Suspended mass with non-radioactive LBE injections in different size bins after 72 hours from accident onset

The reduction of efficacy in the removal of radioactive LBE aerosol from the control volume atmosphere by the introduction of non-radioactive LBE aerosol can be better understood by analyzing the evolution of the overall value (i.e. accounting for both radioactive and non-radioactive particles) of MMD (Figure 5.2).

If particles more than double in size the already suspended particles are injected, only short-term impact is produced on the overall MMD: the injected particles rapidly deposit with limited interaction with the already present radioactive aerosols and the MMD value quickly returns to its pre-injection value. Thus, they have a negligible influence on radioactive aerosol settling.

If relatively small aerosol particles are injected, a long-lasting increase of total MMD is generated. This result in the enhancement of the radioactive aerosol settling, with the reduction up to a factor of 5 of the quantity of radioactive mass suspended after a one-week transient.

The enhanced deposition is expected when aerosol particles grow larger in size, since gravitational deposition velocity is higher for larger particles, as expressed in equation 2.21.

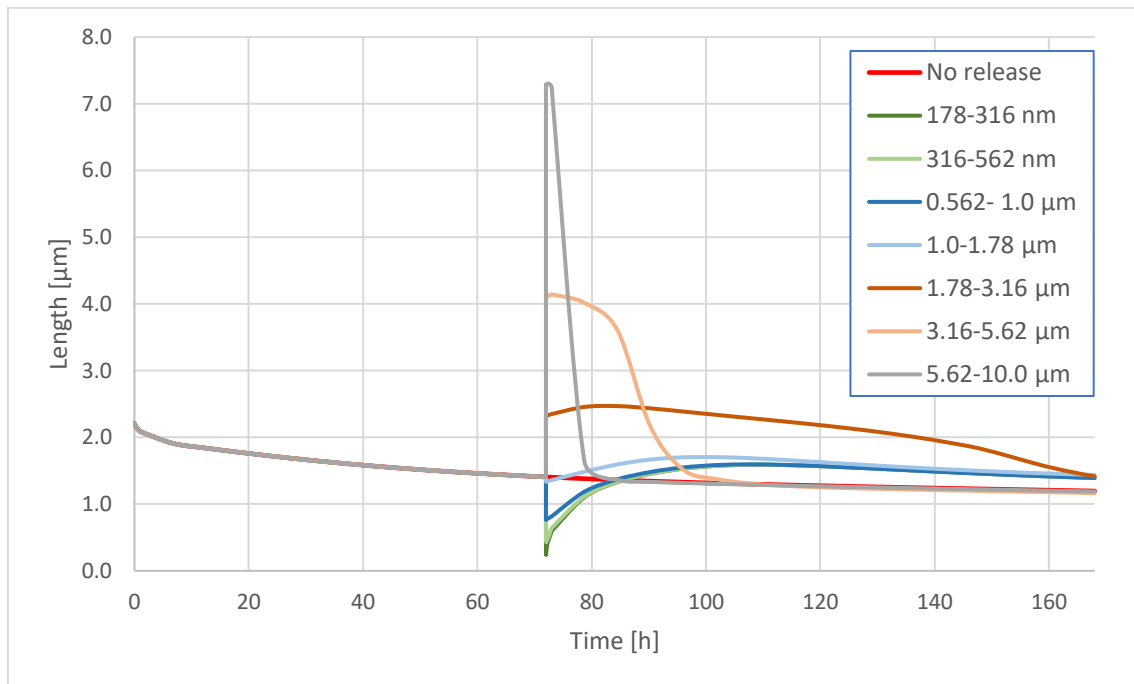


Figure 5.2- Cumulative MMD (considering both radioactive and non-radioactive LBE) for non-radioactive LBE injections at  $t=72h$

The Figures 5.3 and 5.4 display, respectively, the size distribution at the end of the one week transient for the reference case without mitigating injection and for the case postulating the injection of 100 kg of non-radioactive LBE aerosol in the range 1.0-1.78  $\mu m$  72 hours after the initial release of radioactive LBE aerosol.

The injection of non-radioactive LBE aerosol shows to be effective in the removal of the radioactive particles with comparable size to the injected ones, with the reduction of about 75% of the radioactive suspended mass.

Radioactive particles smaller than the injected non-radioactive particles are effectively removed as well.

To visualize the effect on the FOM of a limited variation in size of the injected particles, the final mass distribution obtained by injecting particles in a higher size bin (in the range 3.16-5.62  $\mu m$ ) is shown in Figure 5.5. In this case, the interactions through agglomerating processes between the radioactive and non-radioactive aerosol sources are much more limited: the mass distribution of radioactive material at the end of the transient is similar to the one of the reference case (Figure 5.1, no injection considered). The injected material therefore deposits very quickly and a only negligible fraction of it is still suspended at the end of the transient (i.e. 96 hours after injection).

## 5- Mitigation strategy

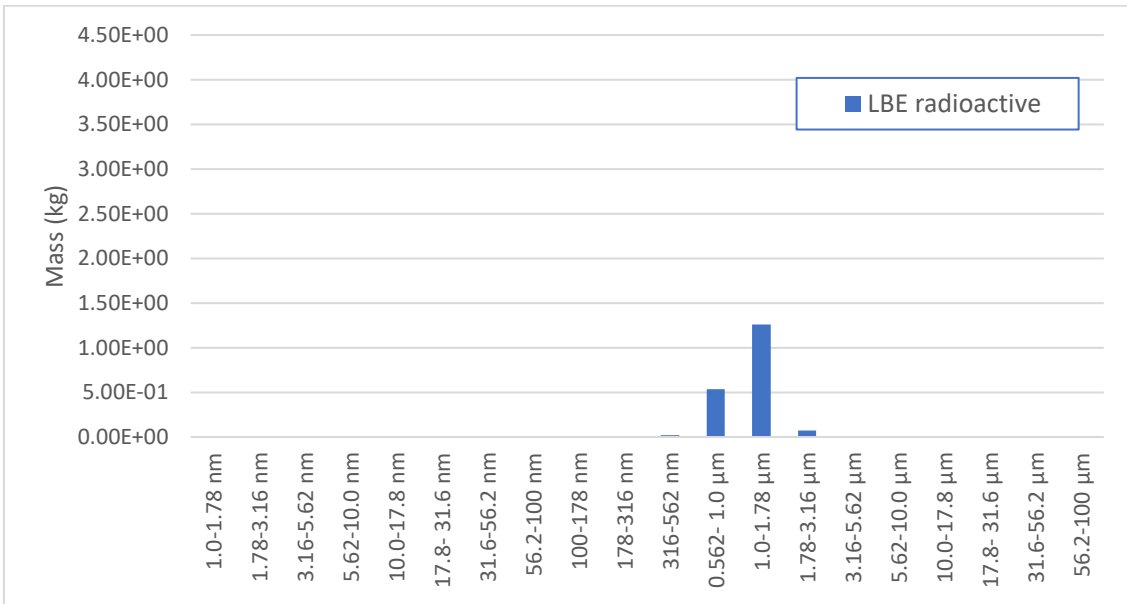


Figure 5.3- Mass distribution one week after accident onset, without mitigation (reference case)

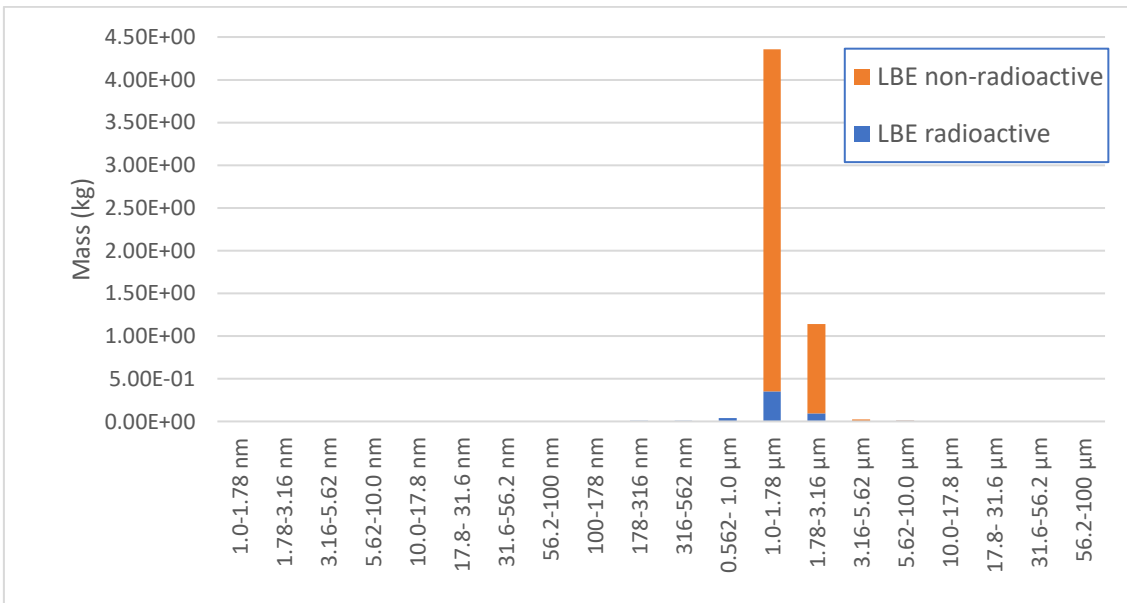


Figure 5.4- Mass distribution one week after accident onset, with the injection of 100 kg of non-radioactive LBE in the range 1.0-1.78 μm after 72h

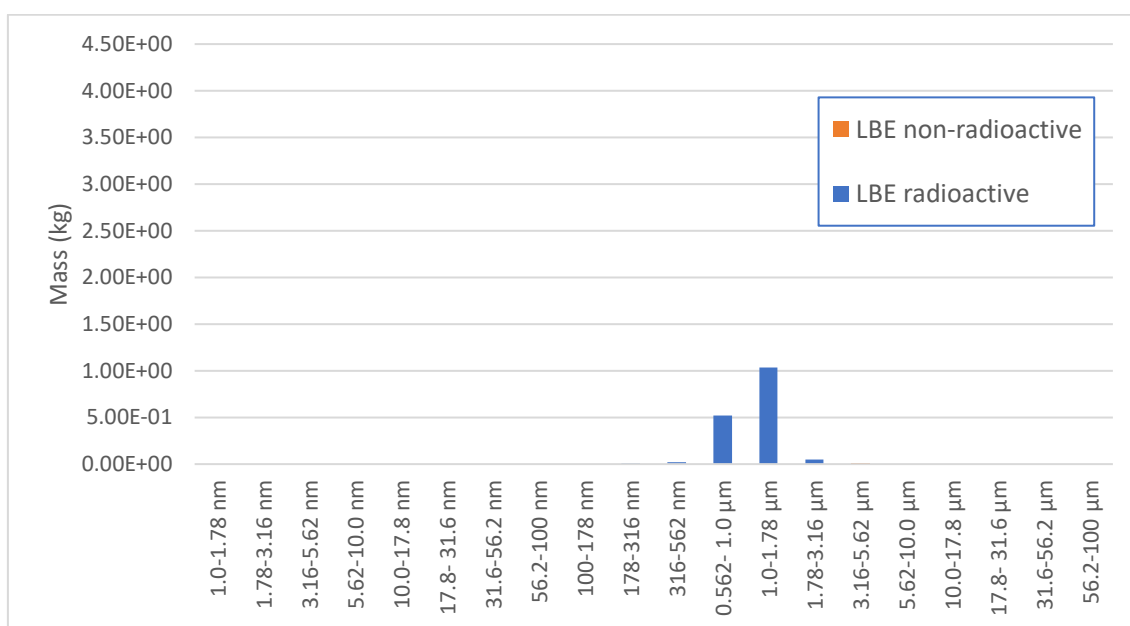


Figure 5.5- Mass distribution one week after accident onset with the injection of 100 kg of non-radioactive LBE in the range 3.16-5.62  $\mu\text{m}$  after 72h

#### 5.4.2 Injection at different times

The injection of a quantity of mass of 100 kg is introduced into different size bins at different times after accident onset. Table 5.3 reports the results of suspended aerosol after a one-week transient obtained for the injection of three monodisperse aerosol sources with different particle size. The postulated times of injection are spaced out of 24 hours starting from the initial radioactive aerosol release up to the sixth day after.

The earliest time of injection, considered at 24 hours, does not result in the most effective removal of suspended activity. Therefore, an earlier start of mitigation is not necessarily beneficial for its effectiveness.

The most effective mitigation is registered for an injection of non-radioactive particles in the range 0.562-1.0  $\mu\text{m}$  48 hours after the accident onset, when the suspended radioactive mass at the end of the one-week transient is more than five and a half times lower than for the unmitigated scenario. The lowest efficiency in the removal of suspended radioactive material is reached with the injection on the sixth day after the release of radioactive material, when a reduction of only about 25% of the suspended radioactive mass can be observed for every size range considered. This may be due to limited time left for the injected aerosol to affect the behaviour of the system before the end of the considered transient. Therefore, a late injection may still produce an effective removal of suspended radioactive material but on a longer time scale.

Once again, the release of smaller particles within the range considered shows to be overall more effective in the mitigation of the suspended activity, whereas the injection

of particles with diameters in the upper part of the considered size range has a comparable effectiveness to the injection of smaller particles only for a late release.

Time of the release of non-radioactive LBE aerosol	Suspended mass of aerosol after 1 week (kg)					
	Size bin in which the non-radioactive aerosol is released					
	0.562- 1.0 $\mu\text{m}$		1.0-1.78 $\mu\text{m}$		1.78-3.16 $\mu\text{m}$	
	Radioactive aerosol	Total aerosol	Radioactive aerosol	Total aerosol	Radioactive aerosol	Total aerosol
24h	0.364	2.894	0.517	2.029	1.214	1.243
48h	0.341	4.648	0.458	3.274	1.026	1.142
72h	0.386	7.783	0.489	5.565	0.963	1.370
96h	0.504	14.052	0.595	10.190	0.977	2.365
120h	0.767	28.218	0.829	20.876	1.084	5.955
144h	1.340	61.776	1.335	49.209	1.380	21.259

Table 5.3- Suspended mass with non-radioactive LBE injections at different times in three different size bins

Figure 5.6 shows the influence of the injections of monodisperse non-radioactive aerosol sources in the range 1.0-1.78  $\mu\text{m}$  at different times on the evolution of the radioactive suspended mass.

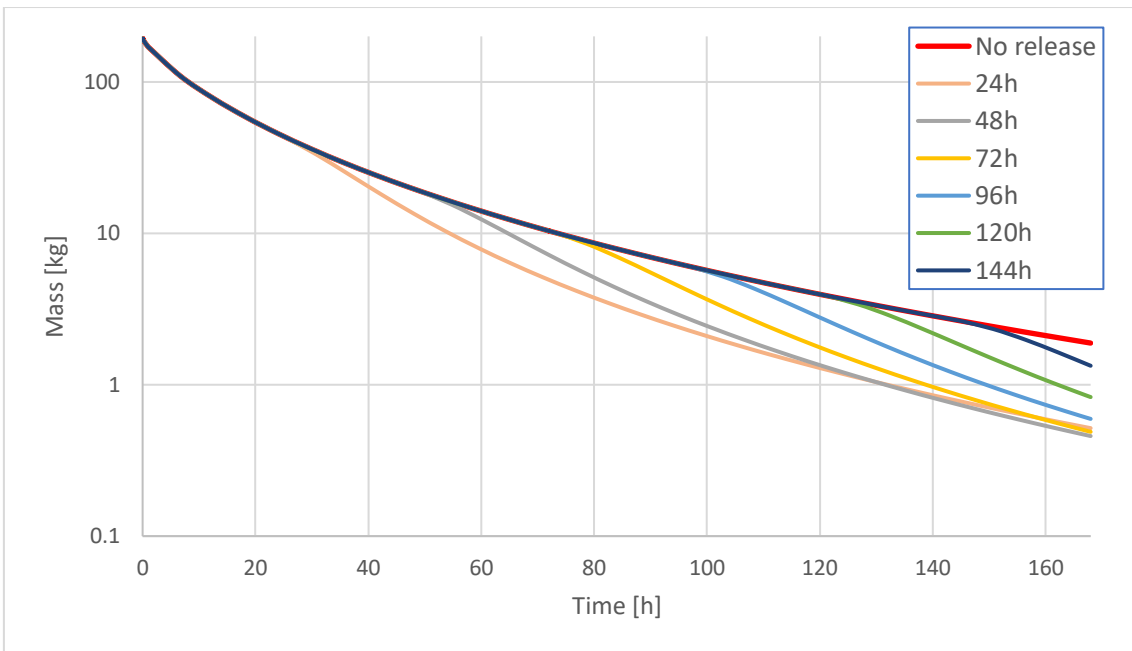


Figure 5.6- Suspended radioactive aerosol mass for the injection at different times in the range 1.0-1.78  $\mu\text{m}$

## 5.5 Conclusions

The injection of non-radioactive LBE results to be a viable strategy for the reduction of suspended radioactive material in the accidental scenario considered.

The injection of a significant quantity (i.e. 100 kg) of aerosol particles in the containment atmosphere can reduce the radioactive mass suspended in the containment atmosphere up to a factor of 5 one week after accident onset.

It can be concluded that, in order to assure an effective mitigation, the size of the injected particles should be comparable or lower than the size of the radioactive ones already present in the containment atmosphere at the time of injection.

Furthermore, the timing of the injection influences the efficacy of the enhancement of deposition of radioactive material. An early intervention does not necessarily translate into less airborne activity in the primary containment; the optimal interval between source term release and onset of mitigation action is found to be 48 hours for the considered characteristics of the aerosol system.

---

# Chapter 6

## Conclusions

---

The proposed study was carried out in the framework of the on-going safety assessment of the MYRRHA facility, a project in development mainly focused on demonstrating the feasibility of the efficient transmutation of high-level nuclear waste in an accelerator-driven system.

The specific initiating event of the accident scenario at study is a leak or break of the LBE conditioning system (LBECS) resulting in the release of radioactive LBE in aerosol form into the Primary Containment of the MYRRHA reactor, with subsequent risk of radioactive releases to the environment.

This study aimed at characterizing the removal of activity from the Primary Containment atmosphere due to natural aerosol deposition processes (i.e. gravitational settling and diffusion by Brownian motion).

The analyses were performed with the aerosol dynamics models implemented in the MELCOR code.

Initially, preliminary considerations were derived from a sensitivity analysis on the initial size and mass of LBE aerosol released. The knowledge derived from this first part was used as a basis for the uncertainty analyses that followed. Additionally, a preliminary study on a possible mitigation strategy was performed.

Conclusions can be drawn from the three distinct parts of the proposed study.

The initial sensitivity analysis aimed at evaluating, for a monodisperse radioactive LBE aerosol source, the influence of initial aerosol size and aerosol mass released on the evolution of the in-containment source term.

The following conclusions can be drawn from the performed sensitivity analyses on LBE aerosol dynamic behaviour:

- The evolution of the suspended aerosol mass in the primary containment atmosphere is independent of the initial particle size for the release of a monodisperse aerosol source with diameters in the range 0.001-1.0  $\mu\text{m}$ .
- Releasing more LBE mass at accident onset is not necessarily conservative. Rather, for the tested quantities, the suspended aerosol mass at the end of a month-

long transient may increase if lower mass is released at the start of the transient. When a shorter time scale is considered, this consideration no longer stands and a higher mass released at accident onset directly translates into higher suspended mass.

- The agglomeration process has a major influence on the aerosol dynamics. The natural deposition process that dominates the aerosol deposition behaviour is gravitational settling.
- Input parameters in aerosol dynamic studies are interacting. It is not possible to isolate the influence of single parameter on the overall behaviour of the system.
- It is therefore difficult to define an envelope case for the safety assessment, which suggests the suitability of an uncertainty analysis approach.

The performed uncertainty analysis aimed at deriving time-dependent values of the suspended LBE aerosol mass in the primary containment atmosphere (the FOM) compliant with the so-called 95/95 criterion and quantify the influence of selected input parameters on the FOM. Values for the FOM that are compliant with 95/95 criterion can be derived, if reliable information is available regarding the variation range and the statistical distribution of the uncertain input parameters, using the coupling between the MELCOR and DAKOTA codes available in the SNAP environment. Awaiting experimental data regarding LBE aerosol source term characterization relevant to the specific conditions at study, the methodology and tools to perform such uncertainty analysis were tested starting from a set of informed assumptions on the parameters that characterize the radioactive aerosol source.

The uncertainty analysis concluded that:

- A time-dependent quantification of the influence of selected uncertain parameter on the FOM can be performed using correlation coefficients. It is highlighted that the high influence of the initial mass of LBE released on the FOM is limited to the first hour after the accident onset. The correlation between the MMD and the FOM is strongest between 1 and 24 hours after accident onset. From 24 hours up the end of the one-week transient the parameters that mainly influence the FOM are the GSD and the dynamic shape factor.
- Overall a significant decrease in the suspended aerosol mass can be achieved by accounting for natural deposition phenomena in the primary containment. A conservative value of the aerosol decontamination factor one week after the initial aerosol release is about 100.

The proposed mitigation strategy for the accident at study is the injection of non-radioactive aerosols to enhance the in-containment natural deposition of radioactive aerosols.

The main conclusions of the preliminary studies for such mitigation strategy are the following:

- Timing is important, an early intervention (i.e. non-radioactive particle injection) does not necessarily translate into less airborne activity in the primary containment.
- The most effective mitigation strategy for the considered characteristics of the system is found to be the injection of particles in the size range 0.562-1.0  $\mu\text{m}$  48 hours after the accident onset. Particles smaller than this size range were not considered in the study.
- Given the above-mentioned size range for the injected particles, their minimum mass necessary to obtain a significant mitigation effect is in the order of 100 kg. Given the above-mentioned size range and total mass for the injected particles, the proposed mitigation strategy can reduce the radioactive mass suspended in the containment atmosphere up to a factor of 5 one week after accident onset, by enhancing the agglomeration of the suspended particles and, consequently, the rate of gravitational deposition.

In the framework of the MYRRHA safety assessment, the obtained results provide useful information for the safety analysis of the initiating event at study.

Preliminary radiological impact assessments can be performed using as input the evolution of the in-containment aerosol source term calculated in this study. The additional insight gained into the dynamic behavior of the system and the most relevant uncertain parameters is also valuable in determining the priorities for the LBE aerosol experimental campaign currently on-going at SCK CEN.

# Bibliography

- [1] J. Bongiorno, J. Parsons, M. Corradini and D. Petti, “The Future of Nuclear Energy in a Carbon-Constrained World,” Massachusetts Institute of Technology, 2019.
- [2] International Energy Agency, “Nuclear Power in a Clean Energy System,” IEA Publications, 2019.
- [3] P. Ray and M. Biswal, *Microgrid: Operation, Control, Monitoring and Protection*, Springer, 2020.
- [4] “Accelerator-driven Nuclear Energy,” World Nuclear Association, August 2018. [Online]. Available: <https://world-nuclear.org/information-library/current-and-future-generation/accelerator-driven-nuclear-energy.aspx>. [Accessed 10 June 2021].
- [5] U.S. DOE Nuclear Energy Research Advisory Committee, “A Technology Roadmap for Generation IV Nuclear Energy Systems,” 2002.
- [6] OECD Nuclear Energy Agency for the Generation IV International Forum, “Technology Roadmap Update for Generation IV Nuclear Energy Systems,” 2014.
- [7] International Atomic Energy Agency, “Status of Accelerator Driven Systems Research and Technology Development,” IAEA TECDOC, 2015.
- [8] H. A. Abderrahim, D. De Bruyn, G. Van den Eynde and S. Michiels, “Transmutation of High-level Nuclear Waste by Means of Accelerator Driven System,” *WIREs Energy and Environment*, 2014.
- [9] NEA, “Accelerator-driven Systems (ADS) and Fast Reactors (FR) in Advanced Nuclear Fuel Cycles,” Nuclear Energy Agency- Organisation for Economic Co-operation and Development, 2002.
- [10] A. Krása, “Spallation Reaction Physics,” Nuclear Sciences and Physical Engineering at Czech Technical University, 2010.
- [11] H. A. Abderrahim, D. De Bruyn, M. Dierckx, R. Fernandez, L. Popescu, M. Schyns, A. Strankovskiy, G. Van den Eynde and D. Vandeplassche, “MIRRH Accelerator Driven System Programme: Recent Progress and Perspectives,” *Nuclear Power engineering*, vol. 2, pp. 29-41, 2019.
- [12] Nuclear Energy Agency, “Handbook on Lead-bismuth Eutectic Alloy and Lead Properties, Materials Compatibility, Thermal-hydraulics and Technologies,” Nuclear Energy Agency- Organization for Economic Co-operation and Development, 2015.
- [13] SCK CEN, “MYRRHA Reactor,” [Online]. Available: <https://myrrha.be/myrrha-project/myrrha-reactor/>. [Accessed 28 May 2021].
- [14] L. L. Humphries, B. A. Beeny, F. Gelbard, D. L. Louie and J. Phillips, “MELCOR Computer Code Manuals- Vol. 1: Primer and Users' Guide. Version 2.2.14959,” Sandia National Laboratories, 2019.

- [15] L. L. Humphries, B. A. Beeny, C. Faucett, F. Gelbard, T. Haskin, D. L. Louie and J. Phillips, "MELCOR Computer Code Manuals- Vol. 2: Reference Manual. Version 2.2.14959," Sandia National Laboratories, 2019.
- [16] F. Gelbard, "MAEROS User Manual," Sandia National Laboratories, 1982.
- [17] F. Gelbard and J. H. Seinfeld, "Simulation of Multicomponent Aerosol Dynamics," *Journal of Colloid and Interface Science*, vol. 78, no. 2, pp. 485-501, 1980.
- [18] E. Cunnungham, "On the Velocity of Steady Fall of Spherical Particles through Fluid Medium," in *Proceedings of the Royal Society of London*, 1910.
- [19] B. M. Adams, W. J. Bohnhoff, K. R. Dalbey, M. S. Ebeida, J. P. Eddy, M. S. Eldred, R. W. Hooper, P. D. Hough, K. T. Hu, J. D. Jakeman, M. Khalil, K. A. Maupin, J. A. Monschke and E. Ridgway, "Dakota, A Multilevel Parallel Object-Oriented Framework for Design Optimization, Parameter Estimation, Uncertainty Quantification, and Sensitivity Analysis: Version 6.13 User's Manual," Sandia National Laboratories, 2020.
- [20] C. Geffray, A. Gerschenfeld, P. Kudinov, I. Mickus, M. Jeltsov, K. Kööp, D. Grishchenko and D. Pointer, "Verification and Validation and Uncertainty Quantification," in *Thermal Hydraulics Aspects of Liquid Metal Cooled Nuclear Reactors*, Woodhead Publishing, 2019, pp. 383-405.
- [21] D. P. Loucks and E. van Beek, "Model Sensitivity and Uncertainty Analysis," in *Water Resources Systems Planning and Management*, Springer, 2005, pp. 255-290.
- [22] IAEA, "Safety Reports Series No.5- Best Estimate Safety Analysis for Nuclear Power Plants: Uncertainty Evaluation," International Atomic Energy Agency, 2008.
- [23] K. Jones and D. Vogt, "DAKOTA Uncertainty Plug-ins Users Manual," Applied Programming Technology, Inc., 2018.
- [24] K. Jones, B. Dunsford, J. Rothe, D. Ulshafer, D. Voigt, D. Costa, K. Jacob and D. Smith, "MELCOR Plug-in Users Manual," Applied Programming Technology, Inc., 2020.
- [25] "AptPlot User's Manual," Applied Programming Technology, Inc., 2020.
- [26] F. Mascari, *MELCOR/DAKOTA coupling*, 2020.
- [27] S. S. Wilks, "Determination of Sample Sizes for Setting Tolerance Limits," *The Annals of Mathematical Statistics*, vol. 12, no. 1, pp. 91-96, 1941.
- [28] W. C. Hinds, *Aerosol Technology: Properties, Behavior, and Measurement of Airborne Particles*, Wiley-interscience Publication, 1999.
- [29] S. Jordan, W. Cherdron, J.-C. Malet, R. Rzekiecki and Y. Himeno, "Sodium Aerosol Behavior in Liquid-Metal Fast Breeder Reactor Containments," *Nuclear Technology*, vol. 81, no. 2, pp. 183-192, 1988.
- [30] H. A. Morewitz, R. P. Johnson, C. T. Nelson, E. U. Vaughan and C. A. Guderjahn, "Attenuation of Airborne Debris from LMFBR Accidents," Rockwell International Corp., 1978.

- [31] U. Pujala, A. Kumar, P. Sujatha, V. Subramanian, C. Srinivas and R. Baskaran, “Experimental studies on morphological properties of sodium combustion, fission product, structural material and mixed aerosols in a closed chamber towards fast reactor safety,” *Annals of Nuclear Energy*, vol. 130, pp. 319-330, 2019.
- [32] I. H. Dunbar and J. Fermandjian, “Comparison of Sodium Aerosol Codes,” Nuclear Science and Technology, 1984.
- [33] J. F. van de Vate, W. F. van Leeuwen, A. Plomp and H. Smit, “Morphology and Aerodynamics of Sodium Oxide Aerosol at Low Relative Humidities,” in *Proceedings of the CSNI Specialists Meeting on Nuclear Aerosols in Reactor Safety*, 1980.
- [34] M. Barbe-le Borgne, D. Boulaud, G. Madelaine and A. Renoux, “Experimental Determination of the Dynamic Shape Factor of the Primary Sodium Peroxide Aerosol,” *Journal of Aerosol Science*, vol. 17, no. 1, pp. 79-86, 1986.
- [35] R. O. Gauntt, “Uncertainty Analyses Using the MELCOR Severe Accident Analysis Code,” in *Workshop proceedings evaluation of uncertainties in relation to severe accidents and level-2 probabilistic safety analysis*, 2007.
- [36] W. Zeller, “Direct Measurement of Aerosol Shape Factors,” *Aerosol Science and Technology*, vol. 4, no. 1, pp. 45-63, 1985.
- [37] K. A. Gamble and L. P. Swiler, “, Uncertainty Quantification and Sensitivity Analysis Applications to Fuel Performance Modeling,” in *TOP FUEL 2016: LWR fuels fuels with enhanced safety and performance*, 2016.
- [38] M. I. Jyrkama and M. D. Pandey, “Uncertainty, Sample Size and the 95/95 Tolerance Limit,” in *37th Annual Conference of the Canadian Nuclear Society and 41st Annual CNS/CNA Student Conference*, 2017.
- [39] The MathWorks, “MATLAB- The Language of Technical Computation,” The MathWorks, Inc., 2005.
- [40] U.S. Nuclear Regulatory Commission, “Regulatory Guide 1.157- Best-estimate Calculations of Emergency Core Cooling System Performance,” Office of Nuclear Regulatory Research, 1989.

---

# Appendix A - Treatment of the aerosol size variable in MELCOR

---

For reader's convenience, the definitions used in the following discussion are first summarized:

- **GMMD**: geometric mass mean diameter. It is the mass weighted average diameter defined by the following formula:

$$GMMD = \frac{\sum m_i d_i}{M} \quad (A.1)$$

where  $m_i$  is the mass of all the particles in section  $i$  having midpoint diameter  $d_i$  and  $M$  is the total mass for all sections.

- **AMMD**: aerodynamic mass mean diameter. It is defined as the mass weighted average of the aerodynamic diameter where aerodynamic diameter is the diameter of the unit density sphere that has the same settling velocity as the real particle.

$$AMMD = \frac{\sum m_i d_{a,i}}{M} \quad (A.2)$$

where  $m_i$  is the mass of all the particles in section  $i$  having midpoint aerodynamic diameter  $d_{a,i}$  and  $M$  is the total mass for all sections.

- **MMD**: mass median diameter. It is defined as the diameter for which half the mass is contributed by particles larger than the MMD and half by particles smaller than MMD.

$$0.5 \cdot M = \sum_i^{MMD} m_i \cdot n_i \quad (A.3)$$

where  $m_i$  is the mass of all the particles in section  $i$ ,  $n_i$  is number of particles in section  $i$  and  $M$  is the total mass for all sections.

- **CMD**: count median diameter. It is defined as the diameter for which one-half of the total number of particles are smaller and half-one are larger.

$$0.5 \cdot N = \sum_i^{CMD} n_i \quad (A.4)$$

where  $n_i$  is number of particles in section  $i$  and  $M$  is the total mass for all sections.

The MELCOR code, within the RadioNuclide Package, allows for the introduction of an aerosol source (MELCOR input record RN1\_AS) [14]. Once an aerosol source is input and it is set to be released in the vapour phase (atmosphere), the additional record RN1\_AS01 is required to define the sectional distribution of the source, which corresponds to the mass distribution in each size bin. This record allows the selection of a specific size distribution among the following ones: uniform source with respect to the logarithmic diameter, lognormal distribution with respect to the logarithmic diameter and ‘sectionbysection’, where the fraction of mass in each size bin has to be specified.

When the lognormal size distribution is selected the code requires the values for the parameter GEOMM and GSD. The GSD is simply defined in the manual as the value of the geometric standard deviation. The definition of the GEOMM parameter in the MELCOR Users’ Guide [14] is unclear. One part of the text describing the use of the RN\_AS01 record seems to suggest that GEOMM is to be interpreted by the code as MMD. Another part of the same text states that GEOMM is interpreted by the code as AMMD, if the input value is greater than zero; if it is less than zero, the absolute value is the geometric number mean diameter.

The AMMD is further defined in the MELCOR Users’ Guide as a function of the GMMD:

$$AMMD = GMMD \sqrt{\frac{\text{Aerosol density}}{\text{Water density}}} \quad (A.5)$$

In order to verify the mass distribution used by MELCOR in its aerosol physics simulations, MATLAB [39] computations of a lognormal mass distributions are performed.

Both MELCOR and MATLAB mass distribution calculations are performed for LBE aerosol with material density 10000 kg/m<sup>3</sup>.

The lognormal count and mass distribution, as all weighted distributions of any lognormal distribution, will be lognormal and have the same shape when plotted on a logarithmic scale.

The peak of the count distribution and mass distribution are described, respectively, by the CMD and the MMD.

The mass distribution will be displaced along the size axis by a constant amount equal to the ratio MMD/CMD, that can be calculated only knowing the GSD.

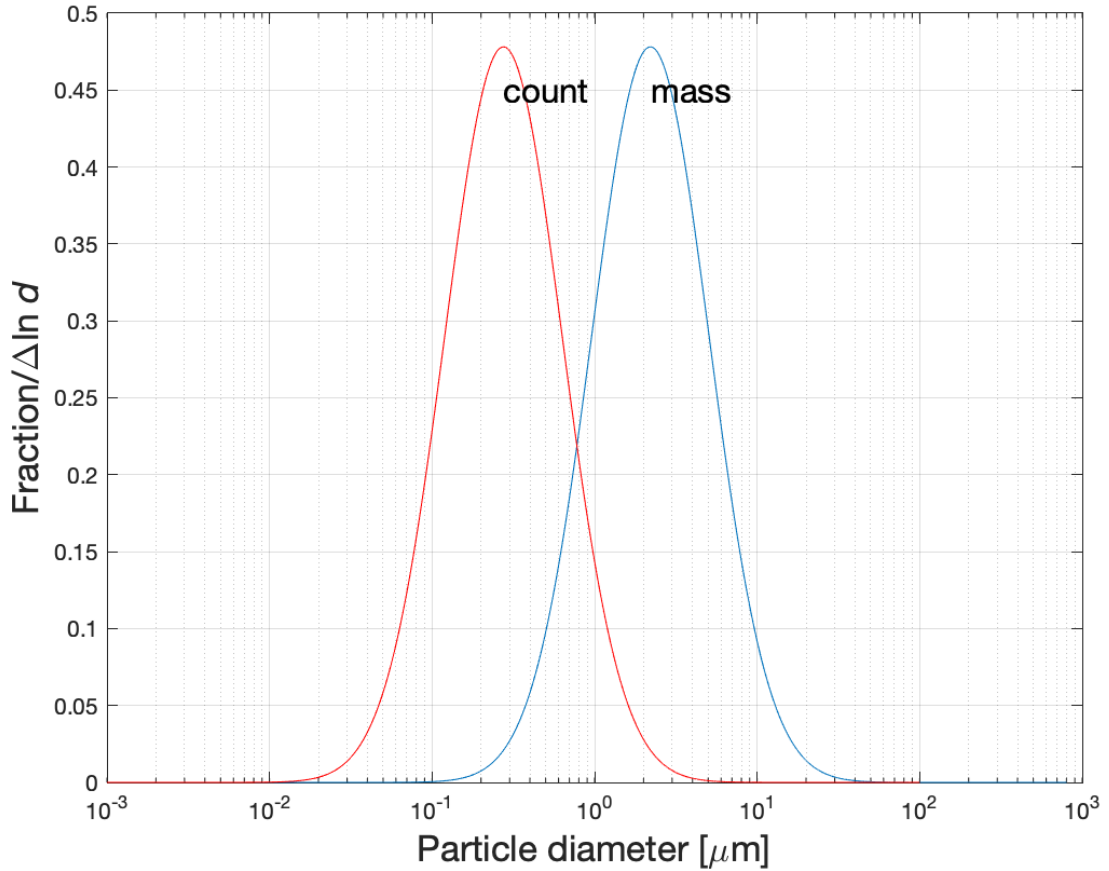


Figure A.1- Count and mass lognormal distributions

The ratio  $MMD/CMD$ , as well as the ratio  $GMMD/CMD$ , can be obtained from conversion equations originally derived by Hatch and Choate (1929) for a given value of  $GSD$  [28].

The conversion equations of interest for the following discussions are:

$$\frac{MMD}{CMD} = \exp(3 \ln^2(GSD)) \quad (A.2)$$

$$\frac{GMMD}{CMD} = \exp(3.5 \ln^2(GSD)) \quad (A.3)$$

Together with the conversion between the  $GMMD$  and  $AMMD$  in equation A.1, equation A.2 and A.3 allow the derivation of any of the averages considered in this discussion starting from one specific average and a value for the  $GSD$ .

With the information presented, it is possible to compare the expected mass distributions with the ones obtained from MELCOR and deduce the correct interpretation of the GEOMM parameter.

A reference mass distribution is first computed with MELCOR, introducing (in the same single-cell model described in section 2.3) an LBE aerosol source of 193 kg and setting the input parameter GEOMM to a value of 2.2  $\mu\text{m}$ , with a GSD of 2.3. Figure A.2 shows the mass distribution recorded immediately after the introduction of the user-defined aerosol source. The mass distribution is displayed as the mass in each size bin that discretizes the size domain.

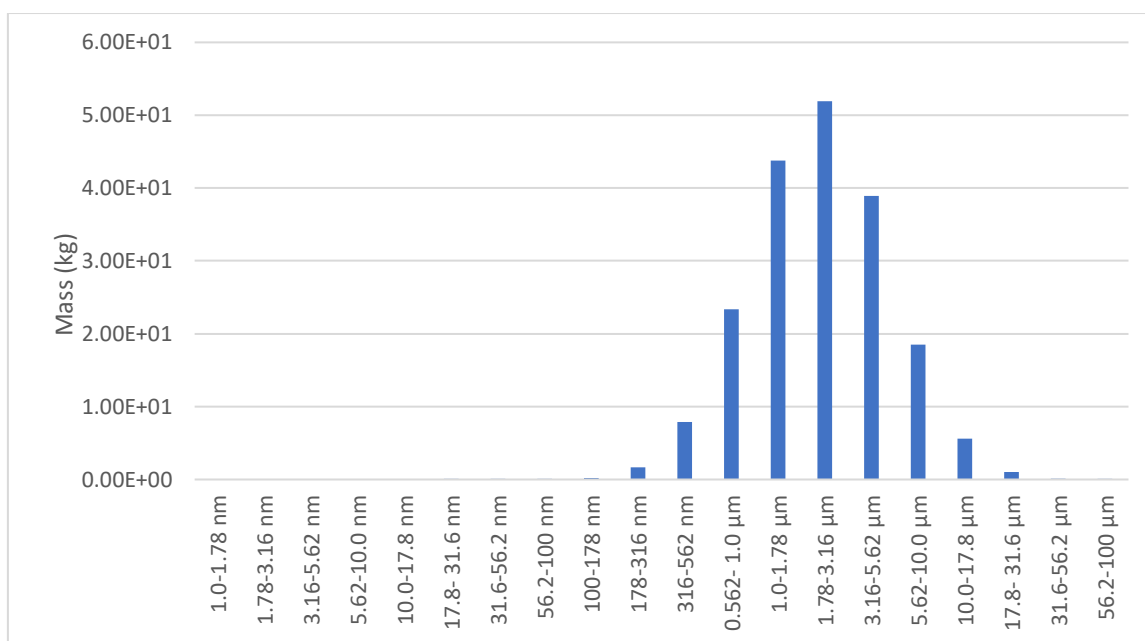


Figure A.2- Mass distribution obtained by MELCOR simulation with GEOMM= 2.2  $\mu\text{m}$

Two mass distributions are then computed with MATLAB, using the same value of the GEOMM parameter as in the MELCOR input and interpreting it as either AMMD or MMD. The same values of GSD and aerosol mass as specified in the MELCOR input are used. The distributions obtained from MATLAB are depicted in Figure A.3.

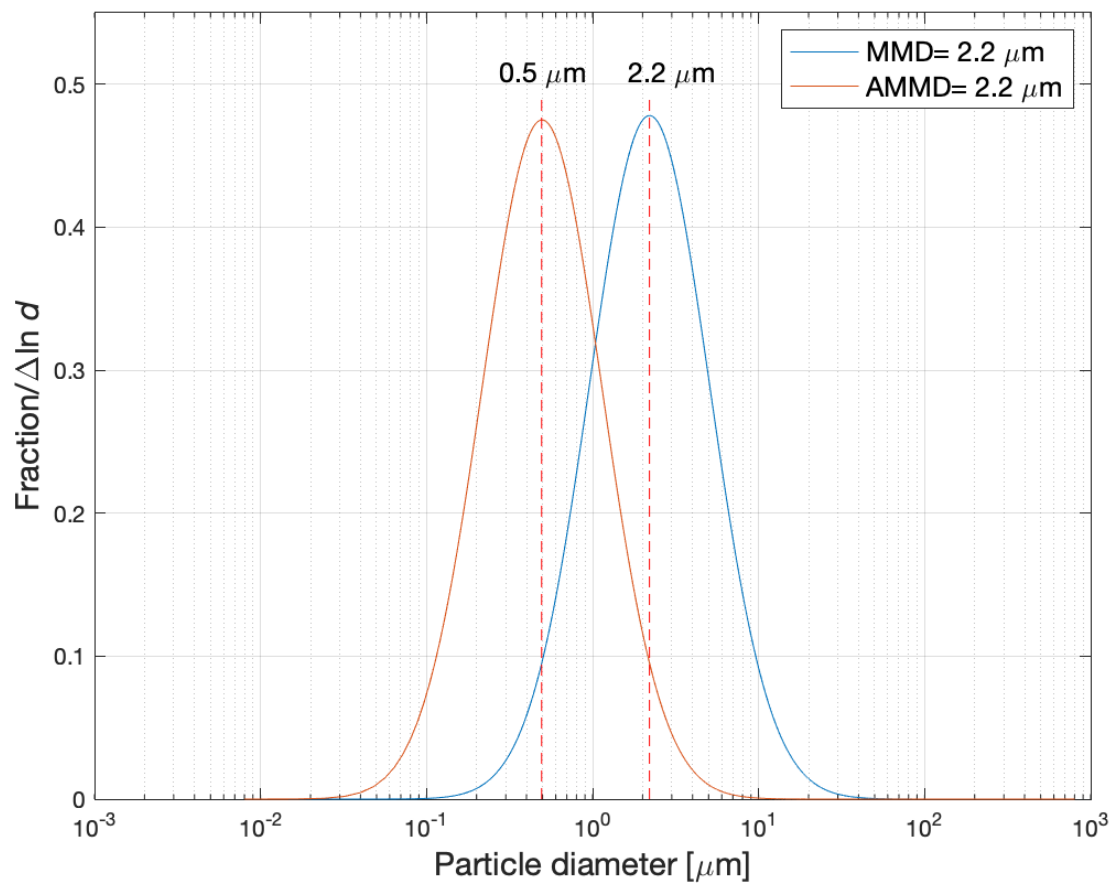


Figure A.3- Mass distributions obtained with MATLAB for an aerosol source with MMD=2.2  $\mu\text{m}$  (blue curve) and with AMMD= 2.2  $\mu\text{m}$  (orange curve)

Since the mass distribution obtained from a MELCOR simulation is displayed as the quantity of mass present in each of the size bins that discretize the size domain, the MATLAB mass distributions are also divided into the same size bins, in order to properly compare the distributions.

The obtained distributions are shown in Figure A.4.

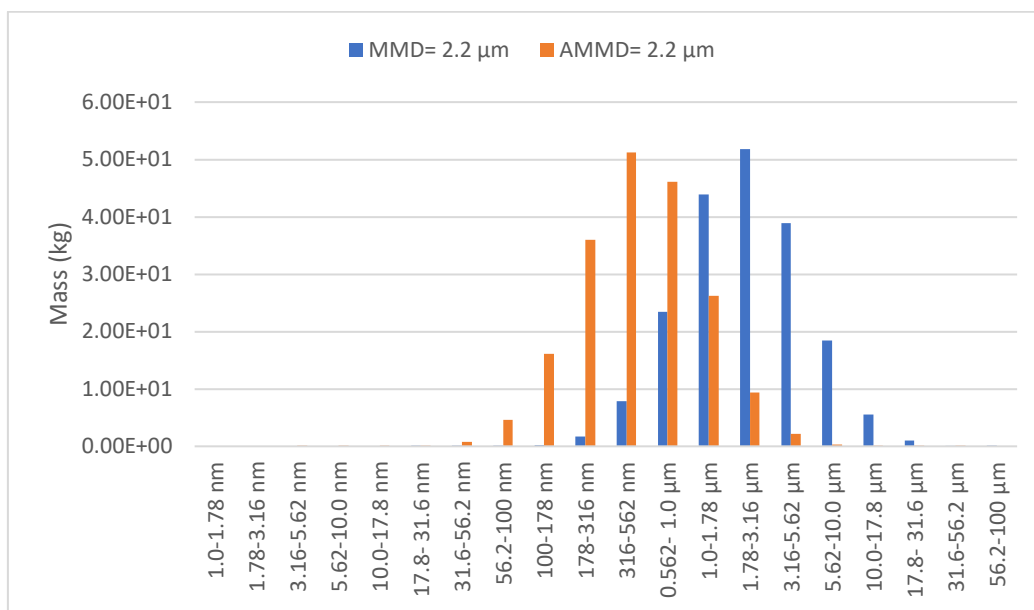


Figure A.4- Discretized mass distributions obtained with MATLAB for an aerosol source with MMD= 2.2 μm (blue histograms) and with AMMD= 2.2 μm (orange histograms)

By comparing Figure A.4 with Figure A.2, it is evident that the value of the GEOMM input parameter is interpreted by MELCOR as MMD rather than AMMD. The aerosol mass distribution obtained from MELCOR using a GEOMM input value of 2.2 μm shows perfect correspondence with the distribution obtained from MATLAB using an aerosol source MMD of 2.2 μm.

It can be concluded that the MELCOR code user's manual wrongly states that a positive value assigned to the GEOMM parameter in the input record RN1\_AS01 is interpreted as the AMMD. A bug report was filed to correct the statement in future code manual revisions.

An additional check is performed for a negative value of GEOMM. According to the manual, the absolute value is interpreted by the code as the geometric number mean diameter. It is important to note that, for a lognormal distribution, the geometric mean diameter is equal to the CMD. The mass distribution obtained for a value of GEOMM equal to -2.2 μm is displayed in Figure A.5.

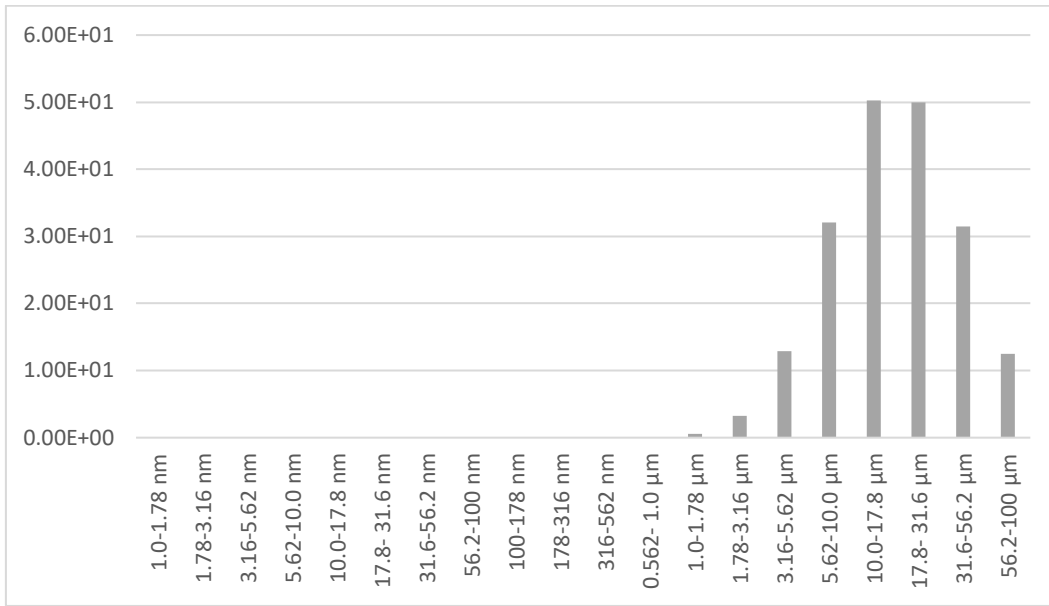


Figure A.5- Mass distribution obtained by MELCOR simulation with GEOMM= -2.2 μm

Similarly as before, the mass distribution is obtained through MATLAB calculations by interpreting the absolute value of the parameter GEOMM as the CMD. The result is presented in Figure A.6, together with the distribution obtained the same value interpreted as the MMD.

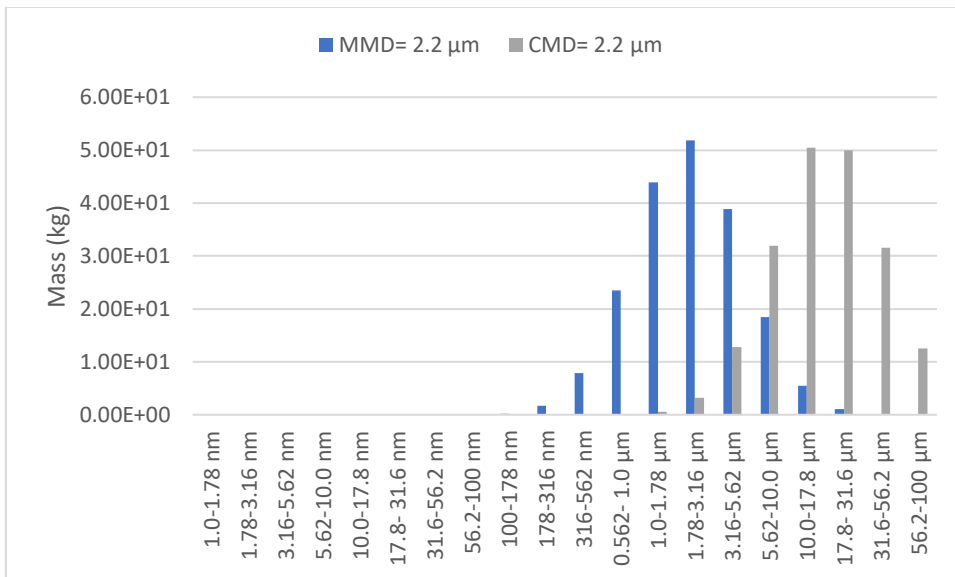


Figure A.6- Mass distributions obtained with MATLAB calculations for the MMD and AMMD

In this instance, perfect correspondence can be found between the mass distribution obtained with MELCOR and MATLAB with the interpretation of the absolute value of the GEOMM as the CMD, as correctly stated in the MELCOR code user's manual.

